Impacts of Sources and Aging on Aerosol Properties in the Marine Boundary Layer Across the Gulf of Maine

P.K.Quinn[1], T.S. Bates[1], D. Coffman[1], T.B. Onasch[2], D. Worsnop[2], T. Baynard[3], J.A. de Gouw[3], P.D. Goldan[3], W.C. Kuster[3], E. Williams[3], J. M. Roberts[3], B. Lerner[3], A. Stohl[4], A. Pettersson[5], E.R. Lovejoy[3], and A.R. Ravishankara[3]

[1]Pacific Marine Environmental Laboratory, NOAA, Seattle, Washington, USA
[2]Aerodyne Research, Inc., Billerica, Massachusetts, USA
[3]Chemical Sciences Division, Earth Systems Research Laboratory, NOAA, Boulder, Colorado, USA
[4]Department of Regional and Global Pollution Issues, Norwegian Institute for Air Research (NILU), Kjeller, Norway
[5]Swedish Defense Research Agency, Stockholm, Sweden

Submitted to JGR-Atmospheres
May 30, 2006

Abstract. Measurements were made onboard the NOAA RV *Ronald H. Brown* during the **s**econd New England Air Quality Study (NEAQS 2004) to determine the source of the aerosol in the region and how sources and aging processes affect aerosol chemical composition and optical properties. Using the Lagrangian particle dispersion model FLEXPART in combination with gas phase tracer compounds, local (urban), regional (N.E. U.S. urban corridor of Washington, D.C., New York, and Boston), and distant (midwest industries and North American forest fires) sources were identified. Aerosol measured near the source region (Boston Harbor) had a molar equivalence ratio near one with respect to NH_4^+, NO_3^-, and $SO_4^=$, had a large mass fraction of particulate organic matter (POM) relative to $SO_4^=$, and had relatively unoxidized POM. As distance from the source region increased, the aerosol measured in the marine boundary layer became more acidic, had a lower POM mass fraction, and the POM became more oxidized. The relative humidity dependence of light extinction reflected the change in aerosol composition being lower for the near-source aerosol and higher for the more processed aerosol. A factor analysis performed on a combined data set of aerosol and gas phase parameters showed that the POM measured during the experiment was predominantly of secondary anthropogenic origin.

1. Introduction

The second New England Air Quality Study (NEAQS 2004) took place as part of the multi-platform International Consortium for Atmospheric Research on Transport and Transformation (ICARTT) activity during July and August, 2004. NEAQS 2004 focused on emissions and meteorological and chemical processes that impact air quality and climate forcing in the New England region. During the experiment, the NOAA RV *Ronald H. Brown* made several transits along the coasts of Massachusetts, New Hampshire, and Maine and across the Gulf of Maine towards Nova Scotia (Figure 1). We focus here on measurements of aerosol chemical composition and gas phase compounds made onboard the ship to address the following scientific questions.

1) What source regions across North America impact the marine boundary layer along the NE U.S. coast and across the Gulf of Maine? Local sources along the coast include urban, industrial, and biogenic emissions. The study area also is subject to regional emissions from the NE urban corridor (including Washington, D.C., New York City, and Boston) [*Merrill and Moody,* 1996]. Distant sources include industrial emissions from the Ohio River Valley and forest fire emissions from western and northern North America [e.g., *Wotawa and Trainer,* 2000]. Understanding how different sources impact aerosol loadings, composition, and optical properties is essential for successfully mitigating the haze that impairs New England's air quality and for understanding regional climate forcing in the northeastern U.S.

2) What are the sources of particulate organic matter (POM) in New England? POM can make up a large fraction of the submicrometer aerosol mass in this region [*Quinn and Bates,* 2003; *Bates et al.,* 2005] and impact aerosol optical properties [*Quinn et al.,* 2005]. Yet little is known about its sources and composition. Simultaneous measurements of gas phase source tracer species and POM concentrations are used to determine the source of the majority of the POM measured during the experiment. This information is a required step in determining POM visibility and climate impacts as well as possible strategies for reducing emissions.

3) How are marine boundary layer aerosol composition and optical properties affected by source region and subsequent aging processes? The mobility of the ship allowed for sampling near coastal sources as well as downwind across the Gulf of Maine. Often, the

ship traveled downwind in the shallow stable marine boundary layer which minimized mixing from aloft [*Angevine et al.*, 2004]. Under these conditions, the continental air masses that were sampled reached the ship with no additional input of urban, industrial, or terrestrial aerosol source material. In other cases, the ship encountered air masses that had been entrained from the upper troposphere into the remote marine boundary layer. These conditions allowed for a characterization of aerosol composition for different sources and aging processes.

The aerosol measurements that are presented in the context of these questions include aerosol size distributions, chemical composition, light scattering, and the relative humidity dependence of light extinction. Only aerosol particles with aerodynamic diameters less than 1 μm (at 60% RH) are considered in this analysis as this is the size range most likely to be a result of anthropogenic sources and to be transported over long distances. Gas phase measurements used to investigate aerosol sources and processing include volatile organic compounds (VOCs) of anthropogenic and biogenic origin, SO_2, peroxyacetyl nitrates (PANs), O_3, and CO.

2. Methods

2.1. Sample Inlet

Sample air for all aerosol measurements was drawn through a 6-m mast. The entrance to the mast was 18 m above sea level and forward of the ship's stack. The transmission efficiency of the inlet for particles with aerodynamic diameters less than 6.5 μm (the largest size tested) is greater than 95% [*Bates et al.*, 2002]. In addition, the data reported here are based on air that was sampled only when the particle number concentration, the relative wind speed, and the relative wind direction all indicated there was no possibility of contamination from the ship's stack.

2.2. Aerosol Chemical Composition

Concentrations of submicrometer NH_4^+, $SO_4^=$, NO_3^-, and POM were measured with an Aerosol Mass Spectrometer (AMS) (Aerodyne Research Inc., Billerica, MA, USA) [*Jayne et al.*, 2000]. The species measured by the AMS are referred to as non-refractory (NR) and are defined as all chemical components that vaporize at the vaporizer temperature of ~550°C. This includes most organic carbon species and inorganic species such as ammonium nitrate and ammonium sulfate salts but not mineral dust, elemental

carbon, or sea salt. The ionization efficiency of the AMS was calibrated every few days with dry monodisperse NH_4NO_3 particles with the procedure described by *Jimenez et al.*, [2003]. The instrument operated with a beam width probe (BWP) [*Huffman et al.*, 2005] sampling on a 5 min cycle, 2.5 min with the signal blocked by the BWP and 2.5 min with the signal unblocked.

The collection efficiency of the AMS depends on the transmission of particles through the aerodynamic lens (E_L), the efficiency with which particles are focused by the lens and directed to the vaporizer (E_s), and the degree to which particles are vaporized and analyzed versus bounced off the vaporizer (E_B) [*Huffman et al.,* 2005]. The AMS sampled downstream of an impactor with a 50% aerodynamic cut-off diameter of 1 μm. The collection efficiency of the aerodynamic lens, E_L, on the AMS inlet, however, is less than 1 for particles with aerodynamic diameters between 500 nm and 1 μm [*Jayne et al.*, 2000]. Particle losses in this size range were corrected using the fraction of particle mass measured in the 0.5 to 1.0 μm size bins of the differential mobility particle sizer (DMPS) and aerodynamic particle sizer (APS). This factor was then applied to the total AMS mass. The correction added, on average, 18 ± 10% to the AMS total mass.

The shape-related collection efficiency, E_S, depends on the efficiency with which particles are focused by the lens and directed to the vaporizer [*Jayne et al*., 2000; *Huffman et al*., 2005]. Based on the BWP data, there was no indication that this factor was different from one for this data set. The collection efficiency due to particle bounce, E_B, appears to be a function of particle water content and chemical composition [*Allan et al.,* 2004]. Pure ammonium nitrate particles, used in the calibration of the instrument have an E_B of nearly 1 [*Jayne et al.,* 2000]. Particles with a high percentage of ammonium sulfate have an E_B of around 0.5 [*Allan et al.,* 2004]. An E_B of 0.5 is often used when no other chemical information is available. Comparison of the size corrected (E_L) AMS NR sulfate from this cruise with sulfate derived from a particle-into-liquid-sampler coupled to an ion chromatograph (PILS-IC) suggests an E_B that varied from 1 for acidic sulfate to 0.45 for ammonium bisulfate. Therefore, E_B was assigned to each 5 minute sample based on the AMS ammonium to sulfate molar ratio with E_B as a linear function of the ammonium to sulfate molar ratio varying from 0.45 to 1 for ratios of 1 to 0.

A linear regression of hourly averaged transmission and bounce corrected AMS sulfate versus PILS-IC sulfate yielded a slope of 0.98 and an r^2 of 0.95. The linear regression for AMS ammonium versus PILS-IC ammonium yielded a slope of 0.87 and an r^2 of 0.76. The uncertainty in the AMS concentration measurements during NEAQS 2004 was estimated at ± 20%.

2.3. Aerosol light scattering and relative humidity dependence of extinction

Measurements of aerosol scattering were made with an integrating nephelometer (Model 3563, TSI Inc.). The RH was measured in the center of the nephelometer sensing volume using a custom-installed sensor (Vaisala model HMP135Y). A single-stage impactor with a 50% aerodynamic cut-off diameter of 1.0 μm was placed upstream of the nephelometer. Values measured by the nephelometer were corrected for an offset determined by measuring filtered air over a period of several hours. In addition, values were corrected for angular nonidealities of the nephelometer, including truncation errors and nonlambertian illumination using the method of *Anderson and Ogren* [1998]. Values are reported at 550 nm, 0°C, 1013 mb, and 60% RH.

The relative humidity (RH) dependence of light extinction by aerosols was measured with a pulsed cavity ring-down aerosol extinction spectrometer (CRD-AES). Details of the measurement procedure and instrumentation can be found in *Baynard et al.* [2006a]. During NEAQS 2004, a reference cell was operated at constant temperature (36°C) and approximately 30% RH. A second, external cell with a single cavity at 532 nm operated with independent temperature control so that the relative humidity of the cell could be adjusted. Based on simultaneous measurement of extinction at the dry, reference RH and at a higher RH, the RH dependence of extinction at 532 nm, was calculated as follows

$$f_{\sigma ep}(RH, RH_{ref}) = \frac{\sigma_{ep}(RH)}{\sigma_{ep}(RH_{ref})} \quad (1)$$

where RH_{ref} = 30% and RH = 66%. The RH dependence of extinction was determined with a ± 2% precision and $\sigma_{ep}(RH_{ref})$ with a 1% uncertainty for a time resolution of 5 sec.

2.4. Aerosol Size Distributions

Size distributions from 20 to 800 nm in geometric diameter were measured with a differential mobility particle sizer (DMPS, University of Vienna (Resichle) medium length column). Uncertainties in the DMPS-measured size distributions include instrumental errors of particle sizing (± 5%) and counting (± 10%) due to flow instabilities. Number size distributions for the 0.54 to 20 μm aerodynamic diameter size range were measured with an aerodynamic particle sizer (APS, TSI model 3320). Uncertainties for the APS size distribution between 0.54 and 1.0 μm include instrumental counting efficiencies (± 5%) and particle sizing (± 3%). Both instruments were operated at 60 ± 10% RH. Details of the size distribution measurements can be found in *Bates et al.* [2004].

2.5. Gas Phase Compounds

Nonmethane hydrocarbons and oxygenated species were measured by on-line gas chromatography-mass spectrometry (GC-MS) [*Goldan et al.*, 2004; *de Gouw et al.*, 2005]. Samples were collected and analyzed every 30 min. The measurement precision was typically 2% and accuracy was 10%. The detection limit for most compounds was below 1 pptv (parts per trillion by volume).

Details for the measurement of PANS in this study can be found in *Williams et al.* [2000] and *Roberts et al.* [2002] with changes or additions to those methods described below. The measurement was made by capillary GC/ECD with sample loop injection every 5 minutes. An all-PFA Teflon inlet at 1 SLPM flow rate with PAN thermal decomposition and calibration plumbing were fitted to the inlet as described by *Roberts et al.*, [2002]. The instrument response to PAN was calibrated routinely, every 5 hours, using a modified acetone/CO/NO photolysis source which is based on the calibrated NO mixing ratio and known conversion efficiency (93 ± 3%). Prior to the cruise, the photolysis source was compared to a diffusion source consisting of a PAN/tridecane/pentadecane mixture in a pressure, temperature and flow controlled capillary cell. The output of the capillary cell was calibrated using an NOy instrument. The responses of the GC system to the two PAN sources were within 5% of each other. MPAN calibration was based on relative response factors that had been determined in the laboratory and that have been consistent within 5% over several different field

campaigns. The detection limit for MPAN was 10 pptv and the overall uncertainty was ± (10 pptv + 20%).

A TECO 49 analyzer was used to measure ozone. The analyzer was calibrated to a NIST traceable analyzer prior to the experiment. Data were recorded as 1 min averages and then averaged into 30 min intervals for comparison to the VOC measurements.

SO_2 was measured with a Thermo Environmental Instruments Model 43C Trace Level Pulsed Fluorescence SO_2 Analyzer. Details of the sample inlet and calibration method can be found in *Bates et al.* [2005].

CO was measured with a modified AeroLaser GmbH [Garmisch-Partenkirchen, Germany] AL5002 Ultra-Fast CO analyzer, a commercially-available vacuum-UV resonance fluorescence instrument [*Gerbig, et al.,* 1999]. For the campaign, data were collected at 1 Hz and averaged to a 1-minute resolution; the total uncertainty is estimated at 3%, with a limit of detection of 1.5 ppbv.

2.6. FLEXPART

FLEXPART, a Lagrangian particle dispersion model [*Stohl et al.,* 1998; *Stohl and Thomson,* 1999], was used to determine the origin of aerosols that had undergone transport to the ship. FLEXPART was driven with model-level data from the European Centre for Medium-Range Weather Forecasts (ECMWF) at a resolution of 0.36° x 0.36° in the area of interest here. The ECMWF model has four levels in the lowest 100 m of the atmosphere and can resolve some of the structure of the marine boundary layer. However, when the lowest part of the marine boundary layer is strongly decoupled from the flow above, as often occurs over the cold waters of the Gulf of Maine, excessive vertical mixing may occur in FLEXPART. Nevertheless, the results show that FLEXPART captures the variability of long-lived tracers along the ship track reasonably well.

Backward simulations were done along the ship cruise track every hour or whenever its position changed by more than 0.1 degrees. The backward simulations were done with full turbulence and convection parameterizations [*Seibert and Frank,* 2004; *Stohl et al.,* 2003]. Every simulation consists of 40,000 particles (small air parcels) released in the volume of air sampled and transported back in time, from which a so-called potential emission sensitivity (PES) function was calculated. The word "potential" here indicates

that this sensitivity is based on transport alone, ignoring removal processes that otherwise would reduce the sensitivity. The value of the PES function (in units of s kg^{-1}) in a particular grid cell is proportional to the particle residence time in that cell. It is a measure of the simulated mixing ratio at the receptor that a source of unit strength (1 kg s^{-1}) in the respective grid cell would produce. Of special interest is the PES distribution at altitudes where emissions are likely to occur (here, the lowest 150 m were used for anthropogenic emissions). Folding (i.e., multiplying) the PES footprint with the distribution of actual emission flux densities (in units of kg m^{-2} s^{-1}) from the inventory yields a so-called potential source contribution (PSC) map, that is the geographical distribution of sources contributing to the simulated mixing ratio at the receptor. Spatial integration of the PSC map gives the simulated mass mixing ratio at the receptor. Time series of the simulated mixing ratios, obtained from series of backward simulations, are presented. Since the backward model output is available with a daily resolution, the timing of the contributing emissions is also known. This product reveals the composite age of tracers reaching the ship and, hence, serves as a "FLEXPART transport clock." As tracers we use CO, NO_2, and SO_2, whose emissions over most of North America are taken from *Frost et al.* [2006]. Biomass burning CO emissions are also used and are based on the daily areas burned per province in Canada and the U.S. provided by the Center for International Disaster Information and MODIS hot spot data.

3. Results - Impact of Sources and Processing on Aerosol Chemical Composition

Figure 1 shows the entire cruise track of the ship during NEAQS 2004. Highlighted along the cruise track are the case studies that will be considered in terms of source of the aerosol and impacts of the source on aerosol composition and optical properties. The case studies include periods spent in Boston Harbor and Blue Hill Bay. The latter is located along the coast of Maine in Acadia National Park. Several transits were made across the Gulf of Maine tracking pollution plumes coming from the NE urban corridor (Washington, D.C., New York, and Boston). In addition, plumes that had undergone longer range transport to the E. Gulf of Maine were sampled. For each case study the location of the ship, the source of the air mass sampled, the chemical composition of the aerosol, and the source of the POM will be discussed. Reported parameters describing

aerosol chemical composition include acidity, as defined by the molar equivalence ratio of NH_4^+ to NO_3^- plus $SO_4^=$ or

$$ER = C_{NH4+} / (C_{NO3-} + 2 \times C_{SO4=}) \quad (2),$$

where C_{NH4+}, C_{NO3-}, and $C_{SO4=}$ are the measured concentrations of the respective non-refractory (NR) ion in μmol m^{-3}. Also reported is the relative amount of NR POM and $SO_4^=$ or

$$F_O = C_O/(C_O + C_S) \quad (3)$$

where C_O and C_S are the measured mass concentrations in μg m^{-3} of NR POM and NR $SO_4^=$, respectively. The degree of oxidation of the POM based on the fraction of the total POM at mass/charge (m/z) 44 is given by the m44/POM ratio. The peak at m/z 44 occurs in the mass spectra of heavily oxidized organic species such as di- and poly carboxylic acids [*Allan et al.*, 2004].

The fraction of total S present as $SO_4^=$ is given by

$$F_{SO4} = C_{SO4=} / (C_{SO2} + C_{SO4=}) \quad (4)$$

where $C_{SO4=}$ and C_{SO2} are the measured concentrations in μmol m^{-3}. Although not a completely conservative tracer due to different loss processes for $SO_4^=$ and SO_2, F_{SO4}, can indicate the relative age of the sampled aerosol. Relatively young aerosol has a low ratio due to insufficient time for conversion of SO_2 to $SO_4^=$ via gas and aqueous phase oxidation processes. As the aerosol ages and more SO_2 is converted to $SO_4^=$, the ratio increases. Table 1 compares ER, F_O, m44/POM, and F_{SO4} for each case study.

Origin of the POM for each case study is probed using gas phase species that have a primary anthropogenic, secondary anthropogenic, or biogenic source. Acetylene is a primary anthropogenic volatile organic carbon (VOC) emitted from automobile exhaust [*Harley et al.*, 1992] and is often used as an indicator of urban emissions. It has a lifetime

on the order of a few weeks. Toluene and benzene are shorter-lived primary anthropogenic VOCs emitted from automobile exhaust. Toluene has a greater reactivity with respect to OH than does benzene. As a result, assuming minimal mixing of air masses of different origins, the measured toluene to benzene ratio decreases with time from emission and can be used to give an indication of the photochemical age of the air mass [*Roberts et al.,* 1984].

Alkyl nitrates such as ethyl nitrate and iso-propyl nitrate are not directly emitted into the continental atmosphere but instead are formed in the atmosphere from the oxidation of other VOCs emitted in urban centers. As such, they are considered to be secondary anthropogenic VOCs.

Isoprene and monoterpenes are highly reactive VOCs that are directly emitted into the atmosphere from vegetation. When isoprene reacts with OH, the first stable products are methyl vinyl ketone (MVK) and methacrolein [*Atkinson,* 2000] both of which are also high highly reactive with respect to OH. Peroxymethacrylic nitric anhydride (MPAN) is produced from oxidation of methacrolein [*Roberts et al.,* 1998; 2002]. Here, MVK, and methacrolein are used as tracers of first generation biogenic emissions. MPAN is used as an indicator of second generation biogenic oxidation products.

Acetonitrile is a relatively long-lived VOC tracer for biomass and biofuel burning [*Lobert et al.,* 1990; *Bange and Williams,* 2000; *Holzinger et al.*, 2005].

3.1. Local Sources

3.1.1. Boston Harbor. The ship docked at the Coast Guard Pier in Boston Harbor on the night of August 8th to sample urban emissions from Boston as the sun came up and traffic increased the following day. Measurements of aerosol composition and gas phase species were made from 08:00 to 14:00 UTC (04:00 – 10:00 EDT) on the 9th. During this period, the wind was from the NW with an average speed of 3.2 ± 0.64 m sec^{-1} such that the ship was directly downwind of the city. Figure 2a shows the cruise track as the ship entered the harbor and the corresponding increase in toluene concentration. F_O, the fraction of POM + $SO_4^=$ due to POM, was very high averaging 0.91 ± 0.05 (Table 1). The ratio of m44 to POM was low (0.03 ± 0.01) indicating that the POM was relatively unoxidized (Figure 2b). Over the 6 hour period, the concentration of POM decreased by about a factor of two while the concentration of toluene increased from 0.2 to 0.6 ppbv

(Figure 2c). The relatively high toluene to benzene ratio of 2.1 ± 0.4 was typical of an unprocessed urban plume. The lack of correlation between POM and toluene or benzene suggests that the POM was not a result of primary anthropogenic emissions.

3.1.2. Blue Hill Bay. Figure 3a shows the approach of the ship to Blue Hill Bay on August 4th. The ship sat in the Bay overnight and from 04:00 to 10:00 UTC (00:00 to 06:00 EDT) measurements were made of POM and gas phase compounds. During this period, the winds were from the northwest bringing flow from the forest to the ship. The wind speed was light and variable averaging 2.8 ± 1.2 m sec^{-1}. F_o averaged 0.91 ± 0.03 and the m44 to POM ratio was 0.07 ± 0.01 indicating relatively unoxidized POM (Figure 3b). POM concentrations initially decreased during the period and then increased during the last two hours. In contrast, the monoterpene concentrations (sum of α-limonene, α-pinene, and β-pinene) initially increased and then leveled off during the middle portion of the period. MPAN concentrations gradually increased from about 08:00 to 12:00 UTC. Figure 4 shows the correlation between POM and MPAN as well as POM and iso-propyl nitrate. The stronger correlation with iso-propyl nitrate suggests that the POM was of secondary anthropogenic origin rather than of biogenic origin.

3.2. NE U.S. Urban Plumes

During the cruise, four periods were identified as "pollution plume" events based on sub-1 μm scattering levels greater than 50 Mm^{-1} for more than 10 hours. Of these, three are presented here as instances of pollution from the NE urban corridor advecting out over the Gulf of Maine. The origin of the plumes was identified using FLEXPART backward simulations. In Figure 5 the three plumes are identified in the scattering time series. Also shown are typical FLEXPART simulations for each time period.

3.2.1. Plume 7/17 to 7/18. Between 7/17 09:50 and 7/18 10:00 UTC, the ship zigzagged through a plume that in the past day had been over Long Island, NY and then Boston. The FLEXPART footprint shows a plume approaching Long Island from the west and then veering to the northeast over Boston to the ship (Figure 5). In Figure 6a the cruise track is colored as a function of sub-1 μm scattering to give an indication of the width of the plume and when the ship was in the most intense portion. The first, second, and third encounters with the most intense region of the plume occurred about 140, 270, and 340 km from Boston.

The "FLEXPART transport clock" or composite age of anthropogenic tracers reaching the ship is shown for the 7/17 to 7/18 period in Figure 7a. From the beginning of the period to around 00:00 on 7/18, most of the CO, SO_2, and NO_2 was less than 1 day old. After 00:00 the tracer age was about 1 day old with an increasing fraction up to two days old through the end of the period.

F_O varied from 0.42 to 0.74 with the lower values measured in the most intense regions of the plume (Figure 6b). In addition, as the ship moved to the northeast in its zigzag fashion, F_O decreased with distance from the source region. Similarly, the equivalence ratio was lowest in the high scattering portions of the plume and decreased with distance from the source. The decrease in both ratios with distance from the source indicates the progressive oxidation of SO_2 to $SO_4^=$ resulting in a higher $SO_4^=$ mass fraction without an equivalent increase in either POM or NH_4^+. Also shown in Figure 6b is the increase in F_{SO4} with distance from shore confirming the conversion of SO_2 to $SO_4^=$. The m44/POM ratio increased from 0.07 when the plume was encountered at 10:00 on 7/17 to 0.11 when it was encountered at 19:30 the next day indicating that the POM was becoming more oxidized with increased distance from the source region. The overall result was an aerosol composition that changed as the pollution plume was transported downwind from the source region in the marine boundary layer. During the transport the POM mass fraction decreased, the portion of the POM that was oxidized increased, and the acidity increased.

The toluene to benzene ratio was around 1 when the plume was sampled at 10:00 on 7/17 (Figure 6c). By 20:30 the ratio had reached its minimum value of 0.2 indicating a processed urban plume. The iso-propyl nitrate concentration was the lowest during the first encounter of the plume (10:00 on 7/17) and elevated during successive encounters. POM concentrations followed the trend in iso-propyl nitrate indicating that it was of secondary anthropogenic origin.

3.2.2. Plume 7/30. On 7/30 the ship sailed through another plume that was closer to the coast than in the 7/17 - 7/18 case. The FLEXPART footprint shows a plume coming from the west to Boston and then veering north to the ship (Figure 5). This time, the first and second encounters with the most intense regions of the plume occurred about 90 and 170 km from Boston. Figure 8a shows the cruise track through the plume colored as a

function of sub-1 μm scattering. Based on FLEXPART backward simulations, the age of the anthropogenic tracers reaching the ship (CO, SO_2, and NO_2) was primarily less than one day during the first encounter (Figure 7b). During the second plume encounter, although the majority of each tracer was less than one day old, the fraction that was 2 to 3 days old was greater, especially for SO_2.

F_O stayed relatively constant throughout the period even though sub-1 μm scattering ranged from about 80 Mm^{-1} near the coast to up to 150 Mm^{-1} offshore (Figure 8b). There was a slight decrease during the second encounter of the plume when the ship was furthest away from Boston to around 0.6. The average for the entire period was 0.69 ± 0.06 (Table 1). The m44/POM ratio also showed relatively little change over the period averaging 0.07 ± 0.01 and 0.09 ± 0.01 during the first and second plume encounters, respectively. Similarly, the equivalence ratio was relatively constant (0.85 ± 0.20) until the second encounter when it was found to have decreased to a low of 0.54. F_{SO4} was higher during the first and second passes through the plume (0.73 ± 0.08 and 0.61 ± 0.08, respectively) than when the ship transited along the coast in between the plume passes. The higher value during the southern passage relative to the more distant-from-source northern passage may be due to different source regions impacting the plume. Overall, though, F_{SO4} in the 7/30 plume was lower than that measured in the second and third passes through the intense regions of the 7/17-7/18 plume indicating less conversion of SO_2 to $SO_4^{=}$ due to closer proximity to the source regions.

Figure 8c shows the time series of the concentrations of NR POM, toluene, benzene, and iso-propyl nitrate. The toluene to benzene ratio decreased from about 1.8 during the first plume encounter to 0.4 at the end of the period indicating aging of an urban plume with distance from the source region. The NR POM and iso-propyl nitrate concentrations tracked each other being highest in the intense region of the plume and lowest along the coast. Again, the similarity in their trends suggests the POM was of secondary anthropogenic origin.

3.2.3. Plume 8/11 – 8/12. For the 7/17-7/18 and 7/30 NE urban plume cases, the FLEXPART footprint showed the air mass flow coming predominantly from the west and then turning north to the ship. In contrast, for the 8/11 – 8/12 case, the FLEXPART footprint indicates flow coming from the southwest over Washington, DC; Long Island,

NY; and Boston. The ship started this portion of the cruise on 8/11 at 8:10 UTC about 80 km from Boston (Figure 9a). Two transits were made in to the coast followed by a transit along the coast. At 8/11 22:30 the ship stopped near the shore and stayed there through the end of the period. Given the prevailing wind direction and a local wind speed of 7 m sec^{-1}, this location was 33 km and about 1.3 hrs directly downwind of the Salem power plant. The dominant tracer age for CO, SO_2, and NO_2 was less than one day but there was also a contribution from ages between 2 and 4 days (Figure 7c).

Measurements of the sub-1 μm scattering coefficient revealed that the plume was hugging the coast (Figure 9a). Figure 9b and 9c show that each time the ship approached the coast the NR POM and iso-propyl nitrate concentrations increased along with the toluene to benzene ratio. The simultaneous increase in the toluene to benzene ratio and iso-propyl nitrate concentration indicates a plume composed of both younger and older air masses as would be the case for an air mass that had passed over multiple urban centers before reaching the ship. Before the ship reached the waypoint on 8/11 at 22:30, F_{SO4} was relatively stable showing no clear trend with distance from shore. The average value of 0.80 ± 0.09 is indicative of an older air mass since the majority of the S was in the form of $SO_4^{=}$. Similarly, the equivalence ratio of 0.54 ± 0.10 indicated an aerosol that had been processed in the marine boundary layer such that SO_2 had been converted to $SO_4^{=}$ without enough NH_3 available for neutralization. F_O was relatively low (0.36 ± 0.03) for the entire period also suggesting an efficient conversion of SO_2 to $SO_4^{=}$ with no additional significant source of POM in the marine boundary layer. The ratio of m44 to POM averaged 0.11 ± 0.01 for the whole period.

When the ship stopped at 22:30 at the near shore waypoint, there was a marked decrease in F_{SO4} (from 0.80 ± 0.09 to 0.39 ± 0.12) and an increase in the equivalence ratio (from 0.54 ± 0.10 to 0.76 ± 0.09). In contrast, F_O and m44/POM did not change suggesting the presence of a power plant plume embedded in an urban plume.

3.3. Distant Sources

Three case studies are presented detailing encounters with plumes that were transported from outside the NE U.S. region to the ship. FLEXPART backward simulations for these cases are shown in Figure 10.

3.3.1. Plume 7/9. On July 9th the ship was in the eastern Gulf of Maine about 360 km from Boston. Between 15:30 and 19:30 UTC, a plume with sub-1 μm scattering of 80 Mm^{-1} was encountered in an otherwise background aerosol with scattering less than 35 Mm^{-1} (Figure 11a). FLEXPART backward simulations show flow from due west over midwest industrial regions which then turned southwesterly with flow over Washington D.C. and out to the ship (Figure 10). The tracer age for CO, SO_2, and NO_2 during this four hour period ranged from 2 to 4 days (Figure 7d).

Throughout this four hour period and for several hours on each side, F_{SO4} was essentially one indicating that for this isolated plume and the surrounding background aerosol, all S was present as $SO_4^=$ (Figure 11b). Aerosol composition was distinct for the period, however. F_O during the period averaged 0.28 ± 0.03 while values for the preceding and subsequent 2 hours were up to 0.6. The POM was consistently more oxidized during the period (m44/POM of 0.14 ± 0.02) than in the preceding and subsequent hours. The equivalence ratio averaged 0.22 ± 0.06 indicating a highly acidic aerosol. Hence, this aged plume relative to those measured closer to shore had a lower mass fraction of POM, more oxidized POM, and was more acidic. These features are consistent with changes in aerosol composition measured with increasing distance from shore in the N.E. U.S. regional plumes discussed above.

The toluene to benzene ratio during the period was very low (< 0.3) indicating a highly processed urban plume (Figure 11c). Toluene and benzene absolute concentrations, though elevated in the plume, were about an order of magnitude less than in the regional plumes discussed above. Iso-propyl nitrate also was elevated in the plume but about the same order of magnitude as in the regional plumes.

3.3.2. Plume 7/19. On July 18th the ship returned to the eastern Gulf of Maine. Figure 12a shows the cruise track between July 18 12:00 and July 19 04:00 UTC colored as a function of the toluene to benzene ratio. Between 12:00 and 16:00 UTC on the 18th, the ship encountered air with a toluene to benzene ratio around 0.3. FLEXPART backward simulations indicate that the sampled air had come from the northwest across Lake Erie and then from the southwest across Long Island and out to the ship (Figure 10b). The age of anthropogenic American tracers (CO, SO_2, and NO_2) was primarily 1 to 2 days (Figure 7e) which, when compared to the backward simulation, puts the source over the N.E.

U.S. coast. In contrast, 8 hours later (between 00:00 and 4:00 UTC) the toluene to benzene ratio was less than 0.1. FLEXPART simulations show that the air mass had come from the northwest over midwest industrial regions and then from the west over Washington D.C. and out to the ship. The tracer age was 3 to 4 days which puts the source region over the Ohio River Valley. The Ohio River Valley source is consistent with the very high ratio of simulated SO_2/CO tracer concentrations for this part of the plume. There is evidence of subsidence in the FLEXPART simulation suggesting that the sampled air came from the Ohio River Valley and subsided to the surface shortly before reaching the ship.

The aerosol composition is different for these two periods reflecting the difference in transport, processing times, and dominant sources. During both periods, F_{SO4} was near unity verifying the relatively old age of the sampled air masses (Figure 12b and Table 1). During the 7/18 12:00 – 16:00 period, F_O averaged 0.49 ± 0.04 compared to 0.30 ± 0.02 for the 7/19 00:00 – 4:00 period. In addition, during the period with the photochemically older air mass, the aerosol was more acidic (0.15 ± 0.06) and the POM more oxidized (0.17 ± 0.02). The comparison of the aerosol composition during these two periods confirms what has been reported throughout this paper. As aerosol is transported from the continental source region out over the Gulf of Maine, it becomes more acidic, the POM mass fraction decreases, and the POM becomes more oxidized. Table 1 shows the progression of these chemical parameters for local, regional, and long distance source regions. The most acidic and oxidized aerosol was measured during the 7/19 00:00 – 4:00 period.

3.3.3. Forest fires 7/14. On 7/14, while moving into Boston Harbor, enhanced levels of acetonitrile were measured. Figure 13a shows that as the ship entered the harbor the wind was from the east and acetonitrile concentrations increased up to 200 pptv. FLEXPART backward simulations for this period show flow from the southeast that had been over western North America 8 to 11 days prior to reaching the ship (Figure 14a). The FLEXPART forest fire CO source contribution shows fire activity in this region of North America at the same time (Figure 14b). In addition, the trend in POM followed that in acetonitrile indicating a forest fire source (Figure 13c).

The aerosol composition during this period was different from that sampled in the eastern Gulf of Maine. Values of F_O were much higher averaging 0.86 ± 0.04 (Figure 13b and Table 1). Similar to the aerosol sampled in the eastern Gulf of Maine, however, the POM was oxidized; the average m44/POM ratio was 0.14 ± 0.04. High organic mass fractions also were observed by the aircraft (NOAA P3) when forest fire plumes were sampled during the experiment [A. *Wollny pers. commun.*,, 2006]. The equivalence ratio was very high averaging 0.93 ± 0.42. The high values could have been due to the availability of continental NH_3 for the neutralization of $SO_4^=$ as the plume crossed the country or to elevated levels of NH_3 produced by the forest fires themselves [*Trebs et al.*, 2004].

4. Results – Source of POM

In almost all of the case studies described above, the NR POM time series trend corresponded to that of iso-propyl nitrate suggesting that the POM had a secondary anthropogenic origin. A factor analysis was performed to further investigate the dominant source of the POM measured in the NEAQS 2004 region. Factor analysis often is used to separate chemical species into different factors or source groups based on the covariance of their concentrations [*Sweet and Vermette,* 1992; *Lamanna and Goldstein,* 1999; *Millet et al.,* 2005]. Chemical species with a high degree of covariance are grouped together into factors. The analysis was performed using a principal component method with varimax rotation (SYSTAT 11, SYSTAT Software, Inc.) based on the variables listed in Table 2. These variables include gas phase compounds of primary anthropogenic, secondary anthropogenic, biogenic, and biomass burning origin and aerosol chemical species. Gas phase compounds of distinct origin were used to assign source categories to the statistically determined factors. Thirty-minute averaged data were used. Omitting periods when not all parameters were available left 56% of the cruise data set for the analysis. Results are shown in Table 2.

Four factors explained 83% of the total variance. The addition of more factors failed to explain more than a few additional percent of the variance. Factor 1, which explained 41% of the total variance, was populated with primary anthropogenic VOCs found in urban emissions. These compounds included hexane, benzene, toluene, and acetylene, all of which are associated with motor vehicle use. In addition, methyl-t-butyl ether

(MTBE), which is used as a gasoline additive, had a high loading in this factor. Photochemical age calculated from the measured toluene to benzene ratio using the method of *Roberts et al.* [1984] had a relatively high negative loading indicating a negative correlation with the other parameters in the factor. The only aerosol parameter associated with this factor was m/z 57 which is a mass fragment that is found in primary organic particles emitted by motor vehicles [*Allan et al.,* 2003].

Factor 2 explained an additional 24% of the total variance. The gas phase species in this factor included ethylnitrate, iso-propyl nitrate, and O_3 which are all a result of photochemical processes. This factor is labeled "secondary anthropogenic" as these alkyl nitrates are formed from the oxidation of other anthropogenic VOCs. All of the aerosol species included in the factor analysis (NR $SO_4^{=}$, NO_3^{-}, and POM) had a high loading in this factor. Also present with a very high factor loading was m/z 44, a mass fragment associated with oxidized POM [*Allan et al.,* 2003].

There were several variables that had relatively high loadings in both factors 1 and 2. In factor 1, the highly reactive gas phase species (ethylene and the xylenes) had high loadings in factor 1 (>0.9) and very low loadings in factor 2 (<0.1). The more inert species (CO, acetylene, propane) scored lower in factor 1 (<0.76) and had a significant loading in factor 2 (>0.44). These results most likely reflect the fact that the progression of an air mass from "primary" to "secondary" is a gradual process. The more inert species are still present by the time many secondary products have formed.

Factor 3 explained an additional 9% of the total variance. It was labeled "biogenic" due to high loadings for methacrolein, MVK, and MPAN. Methacrolein and MVK are isoprene oxidation products with a very short lifetime. MPAN is a longer lived product resulting from the oxidation of methacrolein (>1 day at the temperatures during the experiment). Hence, the factor contains both first and second generation biogenic oxidation products. It does not have a significant loading for POM, however (0.15) indicating that in this region and for the time of the experiment the POM did not have a significant biogenic source. Factor 4 explained 8% of the total variance. Because of the relatively high loadings of acetone, acetonitrile, and methanol it was labeled "biomass burning". Again, the loading for POM was low (0.02) most likely due to the infrequent encounters with forest fire plumes during the experiment.

539 The strong association of POM with factor 2 provides further evidence that it was
540 primarily of secondary anthropogenic origin in the NEAQS 2004 region.

541 **5. Results – Impact of Sources and Aging on the Relative Humidity Dependence of**
542 **Light Extinction**

543 Results from previously reported laboratory and field measurements have indicated
544 that POM internally mixed with water soluble salts can reduce the hygroscopic response
545 of the particles thereby decreasing their water content and their ability to scatter light at
546 elevated relative humidities [*e.g., Saxena et al.,* 1995; *Carrico et al.,* 2005, *Baynard et*
547 *al.,* 2006b]. *Quinn et al.* [2005] presented a simplified parameterization describing the
548 impact of POM on the relative humidity dependence of light scattering based on data
549 collected during INDOEX (INDian Ocean Experiment), ACE Asia (Aerosol
550 Characterization Experiment – Asia), and NEAQS 2004. A similar parameterization is
551 presented here based on the NEAQS 2004 data and the relative humidity dependence of
552 light extinction. Here we use the humidity dependence of light extinction rather than the
553 humidity dependence of light scattering because the fast time resolution of the CRD-AES
554 light extinction measurements allows for more direct comparisons with aerosol
555 composition and size distribution data. A thorough discussion of the humidity
556 dependence of light scattering during NEAQS 2004 can be found in *Wang et al.* [2006].

557 Values of the humidity dependence of light extinction, $f_{\sigma ep}(RH, RH_{ref})$, based on two-
558 point RH measurements were calculated from equation (1). All available $f_{\sigma ep}(66,30)$ data
559 for the experiment are plotted against F_O in Figure 15 with the case studies discussed
560 above highlighted. As for INDOEX and ACE Asia, there is a clear decrease in $f_{\sigma ep}(RH,$
561 $RH_{ref})$ with an increase in F_O. A linear fit yields the following function in terms of
562 coefficients ± 1 standard deviation for the region

563

564 $$f_{\sigma ep}(66, 30) = 1.4(\pm 0.005) - 0.3(\pm 0.007)F_O \qquad (5).$$

565

566 Using Mie scattering calculations for two different particle diameters, NH_4^+ to $SO_4^=$
567 molar ratios varying from 0 to 2, and a range of $f_{\sigma ep}(RH, RH_{ref})$ for POM *Quinn et al.*
568 [2005] were able to explain the majority of the observed variability in the $f_{\sigma ep}(RH, RH_{ref})$
569 – F_O dependence for the combined INDOEX-ACE Asia-NEAQS 2004 data set. Through

570 a series of laboratory experiments with varying mixtures of inorganic salts and
571 dicarboxylic acids, *Baynard et al.* [2006b] concluded that the humidity dependence of
572 light scattering of an inorganic/organic aerosol mixture was most sensitive to the aerosol
573 composition and size. The mixing state was found to have a minor influence.

574 The impact of chemical composition on $f_{\sigma ep}(RH, RH_{ref})$ is shown in Figures 16 and 17
575 where F_O is plotted versus $f_{\sigma ep}(RH, RH_{ref})$ and data points are colored as a function of the
576 equivalence ratio and the m44/POM ratio, respectively. Highest values of $f_{\sigma ep}(66,30)$
577 were measured in the eastern Gulf of Maine where the sampled aerosol was the most
578 acidic, had low POM mass fractions, and relatively oxidized POM. Lowest values of
579 $f_{\sigma ep}(66,30)$ were measured in Boston Harbor where the freshly formed aerosol was
580 neutralized (ER near one), had a high POM mass fraction, and where the POM was
581 unoxidized. The NE U.S. plumes that were sampled between Boston and the eastern Gulf
582 of Maine fall between these two end points of freshly formed and aged aerosol.
583 $f_{\sigma ep}(66,30)$ for the NE U.S. Plume (7/17 – 7/18) ranges from 1.1 to 1.2 with the highest
584 values corresponding to more oxidized POM and more acidic aerosol. $f_{\sigma ep}(66,30)$ for the
585 N.E. U.S. Plume (8/11) cover a larger range spanning from 1.16 to 1.31. The highest
586 values correspond to more acidic aerosol but not more oxidized. The forest fire plume is
587 an exception to this continuum as it is aged aerosol but has a low $f_{\sigma ep}(66,30)$ due to its
588 high POM mass fraction.

589 A third parameter that influences $f_{\sigma ep}(66,30)$ is shown in Figure 18 where the symbols
590 are colored as a function of particle surface mean diameter at 60% RH. Given the same
591 chemical composition in a particle composed of a mixture of inorganic and organic
592 compounds, smaller diameter particles have a stronger relative humidity dependence of
593 extinction than larger particles [*e.g., Baynard et al.,* 2006b]. The eastern Gulf of Maine
594 aerosol, in addition to being acidic and having oxidized POM, is of relatively small
595 diameter which may have contributed to the high values of $f_{\sigma ep}(66,30)$. In the other cases,
596 however, $f_{\sigma ep}(66, 30)$ appears to be more driven by aerosol composition than particle size.
597 For example, the higher values of $f_{\sigma ep}(66,30)$ for the N.E. U.S. plume (8/11) correspond
598 to the largest particles measured in the plume. Similarly, the low values of $f_{\sigma ep}(66,30)$ for

599 the Boston Harbor aerosol appear to be more a function of the aerosol composition than
600 the particle size.

601 **6. Conclusions**

602 During NEAQS 2004, measurements were made onboard the NOAA RV *Ronald H.*
603 *Brown* to determine sources of aerosol to the New England region and how those sources
604 and the subsequent processing during transport impacted aerosol chemical and optical
605 properties. Several source regions were identified. These included local emissions from
606 urban centers, regional emissions from the N.E. U.S. urban corridor (Washington, D.C.,
607 New York, and Boston), and distant emissions from midwest industrial regions and North
608 American forest fires.

609 During NEAQS 2002, POM was found to make up 51 ± 19% of the submicrometer
610 aerosol mass at 55% RH [*Quinn and Bates,* 2003]. Based on a strong correlation of POM
611 with iso-propyl nitrate during the 2002 experiment (r^2 = 0.69), *de Gouw et al.* [2005]
612 concluded that a significant fraction of the submicrometer POM was of secondary
613 anthropogenic origin. The same correlation for a combined data set from all case studies
614 presented here (NEAQS 2004) results in a similar coefficient of determination (r^2 = 0.65).
615 In addition, a factor analysis was performed to more thoroughly determine the dominant
616 source of POM in the region. Aerosol and gas phase parameters were included in the
617 analysis and gas phase tracer compounds were used to identify the four factors that
618 explained most of the total variance (primary anthropogenic, secondary anthropogenic,
619 biogenic, and biomass burning). POM had the highest loading in the secondary
620 anthropogenic factor which is consistent with the linear regression results between POM
621 and iso-propyl nitrate from NEAQS 2002 and 2004.

622 Comparing results from the local, regional, and distant sources revealed a consistent
623 pattern of changing aerosol composition with distance from the source as shown in
624 Figures 16 and 17. In Boston Harbor, the aerosol was neutral with an equivalence ratio
625 near one. In addition, the POM mass fraction was high (0.91) and the POM was relatively
626 unoxidized (m/z 44 = 0.03). On the other end of the spectrum, aerosol measured in the
627 eastern Gulf of Maine that was transported from industrial regions in the midwest was
628 acidic (equivalence ratio of 0.15) and had a low POM mass fraction (0.3) with the POM
629 having a high degree of oxidation (m/z 44 = 0.17). Between these two end points was the

aerosol measured close to shore or mid-Gulf where plumes from the N.E. urban corridor were sampled. As the aerosol was processed during transport from the source region in the marine boundary layer, SO_2 was converted to $SO_4^=$ with no additional input of NH_3 to buffer the acid uptake. In addition, with no significant source of POM in the marine boundary layer, the POM mass fraction decreased with distance from the source.

The impact of the changing aerosol composition with distance from source on the relative humidity dependence of extinction also was investigated. The near source neutral, high POM aerosol had lower values of $f_{\sigma ep}(66, 30)$ than did the acidic, low POM aerosol sampled in the eastern Gulf of Maine. One exception to this pattern was the forest fire aerosol that had been transported from Alaska and Canada to the ship. Even though it was aged aerosol, it had a low $f_{\sigma ep}(66, 30)$ since it had maintained its high mass fraction of POM.

Acknowledgements. This work was supported by the Atmospheric Constituents Program of the NOAA Climate Program Office, the NOAA Health of the Atmosphere Program, and the New England Air Quality Study. We thank Drew Hamilton, James Johnson, Theresa Miller, Kristen Schulz and the officers and crew of the *Ronald H. Brown* for logistical, technical, and scientific support. We thank Allen Goldstein and Dylan Millet for helpful discussions. This is PMEL contribution number 2935.

Allan, J.D. et al., Quantitative sampling using an Aerodyne aerosol mass spectrometer: 2. Measurements of fine particulate chemical composition in two U.K. cities, *J. Geophys. Res., 108,* 4091, doi:10.1029/2002JD002359, 2003.

Allan, J.D., et al., Submicron aerosol composition at Trinidad Head, California during ITCT 2K2: Its relationship with gas phase volatile organic carbon and assessment of instrument performance, *J. Geophys. Res., 109,* D23S24, doi:10.1029/2003JD004208, 2004.

Anderson, T.L. and J.A. Ogren, Determining aerosol radiative properties using the TSI 3563 integrating nephelometer, *Aer. Sci. Tech., 29,* 57 – 69, 1998.

Angevine, W.M. et al., Coastal boundary layer influence on pollutant transport in New England, *J. Appl. Met., 43,* 1425-1437, 2004.

Atkinson, R., Atmospheric chemistry of VOCs and NO_x, *Atmos. Environ., 34,* 2063 – 2101, 2000.

Bange, H.W., and J. Williams, New directions: Acetonitrile in atmospheric and biogeochemical cycles, *Atmos. Environ., 34,* 4959 – 4960, 2000.

Bates, T.S., D.J. Coffman, D.S. Covert, and P.K. Quinn, Regional marine boundary layer aerosol size distributions in the Indian, Atlantic and Pacific Oceans: A comparison of INDOEX measurements with ACE-1, ACE-2, and Aerosols99, *J. Geophys. Res., 107*(D19), 10.1029/2001JD001174, 2002.

Bates, T.S. et al., Marine boundary layer dust and pollutant transport associated with the passage of a frontal system over eastern Asia, *J. Geophys. Res., 109,* D19S19, doi:10.1029/2003JD004094, 2004.

Bates, T. S., P.K. Quinn, D.J. Coffman, J.E. Johnson, and A.M. Middlebrook, Dominance of organic aerosols in the marine boundary layer over the Gulf of Maine during NEAQS 2002 and their role in aerosol light scattering, *J. Geophys. Res., 110*, D18, D18202, 10.1029/2005JD005797, 2005.

Baynard, T. et al., Design Considerations and Applications of Cavity Ring-down Aerosol Extinction Spectroscopy, *Journal of Aerosol Science and Technology*, submitted, 2006a.

Baynard, T., R.M. Garland, A.R. Ravishankara, M.A. Tolbert, and E.R. Lovejoy, Key factors influencing the relative humidity dependence of aerosol light scattering, *Geophys. Res. Lett., 33*,L06813, doi:10.1029/2005GL024898, 2006b.

Carrico, C. et al., Hygroscopic growth behavior of a carbon-dominated aerosol in Yosemite National Park, *Atmos. Environ., 38,* 1393 – 1404, 2005.

de Gouw, J.A. et al., Budget of organic carbon in a polluted atmosphere: Results from the New England Air Quality Study in 2002, *J. Geophys. Res., 110*, D16305, doi:10.1029/2004JD005623, 2005.

Frost, G.F., S. A. McKeen, M. Trainer, T. B. Ryerson, J. S. Holloway, D. T. Sueper, T. Fortin, D. D. Parrish, F. C. Fehsenfeld, S.E. Peckham, G.A. Grell, D. Kowal, J., J. Cartwright, N. Auerbach, and T. Habermann, Effects of changing power plant NO_x emissions on ozone in the eastern United States, *J. Geophys. Res.*, in press, 2006.

Gerbig, C., S. Schmitgen, D. Kley, A. Volz-Thomas, K. Dewey, and D. Haaks, An improved fast-response vacuum-UV resonance fluorescence CO instrument, *J. Geophys. Res., 104*, 1699-1704, 1999.

Goldan, P.D., W.C. Kuster, E. Williams, P.C. Murphy, F.C. Fehsenfeld, and J. Meagher, Nonmethan hydrocarbon and oxy hydrocarbon measurements during the 2002 New England Air Quality Study, *J. Geophys. Res., 109*(D21), D21309, doi:10.1029/2003JD004455, 2004.

Harley, R.A., M.P. Hannigan, and G.R. Cass, Respeciation of organic gas emissions and the detection of excess unburned gasoline in the atmosphere, *Environ. Sci. Technol., 26*, 2395 – 2408, 1992.

Holzinger, R. et al., Oxygenated compounds in aged biomass burning plumes over the Eastern Mediterranean: Evidence for strong secondary production of methanol and acetone, *Atmos. Chem. Phys., 5*, 39 – 46, 2005.

Jayne, J.T., D.C. Leard, X. Zhang, P. Davidovits, K.A. Smith, C.E. Kolb, and D.R. Worsnop, Development of an aerosol mass spectrometer for size and composition analysis of submicron particles, *Aersol Sci. Technol., 33*, 49-70, 2000.

Jimenez, J. L., J.T. Jayne, Q. Shi, C.E. Kolb, D.R. Worsnop, I. Yourshaw, J.H. Seinfeld, R.C. Flagan, X. Zhang, K.A. Smith, J. Morris, and P. Davidovits, Ambient aerosol sampling using the Aerodyne Aerosol Mass Spectrometer, *J. Geophys. Res., 108*, 8425, doi:10.1029/2001JD001213, 2003.

Huffman, J.A., J.T. Jayne, F. Drewnick, A.C. Aiken, T. Onasch, D.R. Worsnop, and J.L. Jimenez, Design, Modeling, Optimization, and Experimental Tests of a Particle Beam Width Probe for the Aerodyne Aerosol Mass Spectrometer, *Aerosol Sci. Technol., 39*, 1143–1163, 2005.

Lamanna, M.S. and A.H. Goldstein, In situ measurements of $C_2 - C_{10}$ volatile organic compounds above a Sierra Nevada ponderosa pine plantation, *J. Geophys. Res., 104*, 21,247 – 21,262, 1999.

Lobert, J.M., D.H. Scharffe, W.M. Hao, and P.J. Crutzen, Importance of biomass burning in the atmospheric budgets of nitrogen-containing gases, *Nature, 346*, 552 – 553, 1990.

Merrill, J.T. and J.L. Moody, Synoptic meteorology and transport during the North Atlantic Regional Experiment (NARE) intensive: Overview, *J. Geophys. Res., 101*, 28,903 – 28,921, 1996.

Millet, D.B. et al., Atmospheric volatile organic compound measurements during the Pittsburgh Air Quality Study: Results, interpretation, and quantification of primary and secondary contributions, *J. Geophys. Res., 110*, doi:10.1029/2004JD004601, 2005.

Quinn, P.K. and T.S. Bates, North American, Asian, and Indian haze: Similar regional impacts on climate?, *Geophys. Res. Lett.,* 30 (11), 1555, doi:10.1029/2003GL016934, 2003.

Quinn, P.K. et al., Impact of particulate organic matter on the relative humidity dependence of light scattering: A simplified parameterization, *Geophys. Res. Lett., 32*,L22809, doi:10.1029/2005GL024322, 2005.

Roberts, J.M., F.C. Fehsenfeld, S.C. Liu, M.J. Bollinger, C. Hahn, D.L. Albritton, and R.E. Sievers, Measurements of aromatic hydrocarbon ratios and NO_x concentrations in the rural troposphere: Estimates of air mass photochemical age and NO_x removal rate, *Atmos. Environ., 18,* 2421 – 2432, 1984.

Roberts et al., Measurements of PAN, PPN, and MPAN made during the 1994 and 1995 Nashville Intensives of the Southern Oxidant Study: Implications for regional ozone production from biogenic hydrocarbons, *J. Geophys. Res., 103,* 22,473 – 22,490, 1998.

Roberts, J.M., F. Flocke, C.A. Stroud, D. Hereid, E.J. Williams, F.C. Fehsenfeld, W. Brune, M. Martinez, and H. Harder, Ground-based measurements of PANs during the 1999 Southern Oxidants Study Nashville intensive, *J. Geophys. Res., 107*, 10.1029/2001JD000947, 2002.

Saxena, P., L.J. Hildemann, P.H. McMurry, and J.H. Seinfeld, Organics alter hygroscopic behavior of atmospheric particles, *J. Geophys. Res., 100,* 18755 – 18770, 1995.

Seibert and Frank, Source-receptor matrix calculation with a Lagrangian particle dispersion model in backward mode, *Atmos. Chem. Phys., 4,* 51 – 63, 2004.

Stohl, A., M. Hittenberger, and G. Wotawa, Validation of the Lagrangian particle dispersion model FLEXPART against large scale tracer experiments, *Atmos. Environ. 32*, 4245-4264, 1998.

Stohl, A., and D. J. Thomson, A density correction for Lagrangian particle dispersion models. *Bound.-Layer Met. 90,* 155-167, 1999.

Stohl et al., A backward modeling study of intercontinental pollution transport using aircraft measurements, *J. Geophys. Res., 108,* 4370, doi:10.1029/2002JD002862, 2003.

Sweet, C.W. and S.J. Vermette, Toxic volatile organic compounds in urban air in Illinois, *Environ. Sci. Technol., 26,* 165 – 173, 1992.

Trebs, I., F.X. Meixner, J. Slanina, R. Otjes, P. Jongejan, and M.O. Andreae, Real-time measurements of ammonia, acidic trace gases and water-soluble inorganic aerosol species at a rural site in the Amazon Basin, *Atmos. Chem. Phys., 4,* 967 – 987, 2004.

Wang, W. et al., Aerosol optical properties over the northwestern Atlantic Ocean during NEAQS-ITCT-2004 and the influence of particulate organic matter on aerosol hygroscopicity, *J. Geophys. Res.*, submitted, 2006.

Williams, J., et al., A method for the airborne measurement of PAN, PPN and MPAN, *J. Geophys. Res., 105,* 28,943-28,960, 2000.

Wotawa, G. and M. Trainer, The influence of Canadian forest fires on pollutant concentrations in the United States, *Science, 288,* 324 – 328, 2000.

Table 1. Aerosol Chemical Composition for Case Studies.

Source	ER[b]	F_O[c]	m44/ POM	F_{SO4}[d]
	Local Sources			
Boston Harbor	1.1 ± 0.55	0.91 ± 0.05	0.03 ± 0.01	0.04 ± 0.03
	Regional Sources			
NE U.S. Plume[a] 7/17 – 7/18	0.49 ± 0.12	0.58 ± 0.09	0.10 ± 0.01	0.75 ± 0.13
NE U.S. Plume[a] 7/30	0.83 ± 0.19	0.69 ± 0.06	0.08 ± 0.01	0.57 ± 0.13
NE. U.S. Plume[a] 8/11 – 8/12	0.57 ± 0.13	0.36 ± 0.03	0.11 ± 0.01	0.74 ± 0.18
	Distant Sources			
E. Gulf of Maine 7/9	0.22 ± 0.06	0.28 ± 0.03	0.14 ± 0.02	0.99 ± 0.002
E. Gulf of Maine 7/19	0.15 ± 0.06	0.3 ± 0.02	0.17 ± 0.02	0.97 ± 0.05
Forest Fires 7/14	0.93 ± 0.42	0.86 ± 0.04	0.14 ± 0.04	0.96 ± 0.06

[a]Averages over cruise tracks shown in Figures 6, 8, and 9 for periods when sub-1 μm scattering > 50 Mm^{-1}.

[b]ER = Equivalence Ratio = $C_{NH4+} / (C_{NO3-} + 2 \times C_{SO4=})$ (Equation 2)

[c]$F_O = C_O/(C_O + C_S)$ (Equation 3)

[d]$F_{SO4} = C_{SO4=} / (C_{SO2} + C_{SO4=})$ (Equation 4)

Table 2. Factor Analysis Results Indicating Four Factors: Primary Anthropogenic, Secondary Anthropogenic, Biogenic, and Biomass Burning[a]

	Primary Anthropogenic	Secondary Anthropogenic	Biogenic	Biomass Burning
Parameter	***1***	***2***	***3***	***4***
Acetylene	**0.75**	0.45	0.16	0.21
Benzene	**0.82**	0.44	0.15	0.23
Ethanol	**0.66**	-0.12	0.12	0.47
Ethylbenzene	**0.94**	0.12	0.23	0.18
Ethylene	**0.91**	0.07	0.26	0.15
i-Butane	**0.81**	0.42	0.14	0.19
i-Propanol	**0.78**	0.01	0.20	0.41
MEK	**0.60**	0.51	0.25	0.46
mp-Xylene	**0.93**	0.02	0.21	0.14
MTBE	**0.88**	0.19	0.25	0.11
n_Hexane	**0.89**	0.16	0.18	0.20
o_Xylene	**0.93**	0.03	0.23	0.16
Photochemical age	**-0.59**	0.09	-0.44	-0.11
Propane	**0.77**	0.47	0.12	0.22
Toluene	**0.92**	0.15	0.25	0.17
m/z 57	**0.52**	0.39	0.17	-0.09
CO	**0.61**	**0.62**	0.09	0.26
Ethyl nitrate	0.14	**0.91**	-0.18	0.07
i-Propyl nitrate	0.22	**0.90**	-0.13	0.11
Ozone	-0.39	**0.81**	-0.11	0.14
NR SO4	-0.05	**0.74**	0.15	-0.08
NR NO3	0.56	**0.62**	0.25	-0.07
NR POM	0.35	**0.84**	0.15	0.02
m/z 44	0.09	**0.93**	0.01	0.07
Sub-1 scattering	0.18	**0.87**	0.13	0.05
Acetone	0.36	0.45	0.23	**0.66**
Acetonitrile	0.16	0.06	0.07	**0.71**
Methanol	0.55	-0.06	0.35	**0.67**
Methacrolein	0.57	0.10	**0.72**	0.16
MPAN	0.34	0.08	**0.82**	0.13
MVK	0.51	0.02	**0.74**	0.29
% total variance	41	24	9.3	8.4
% cumulative variance	41	65	73	83

[a]The rotated loading matrix composed of the coefficients of the factors after the varimax rotation. The highest factor loading for each variable is in bold. The sums of squares of the coefficients for each factor equals the variance explained by that factor.

Figure 1. Cruise track of the NOAA RV *Ronald H. Brown* during NEAQS 2004 with case studies highlighted. The yellow dots indicate the location of power plants.

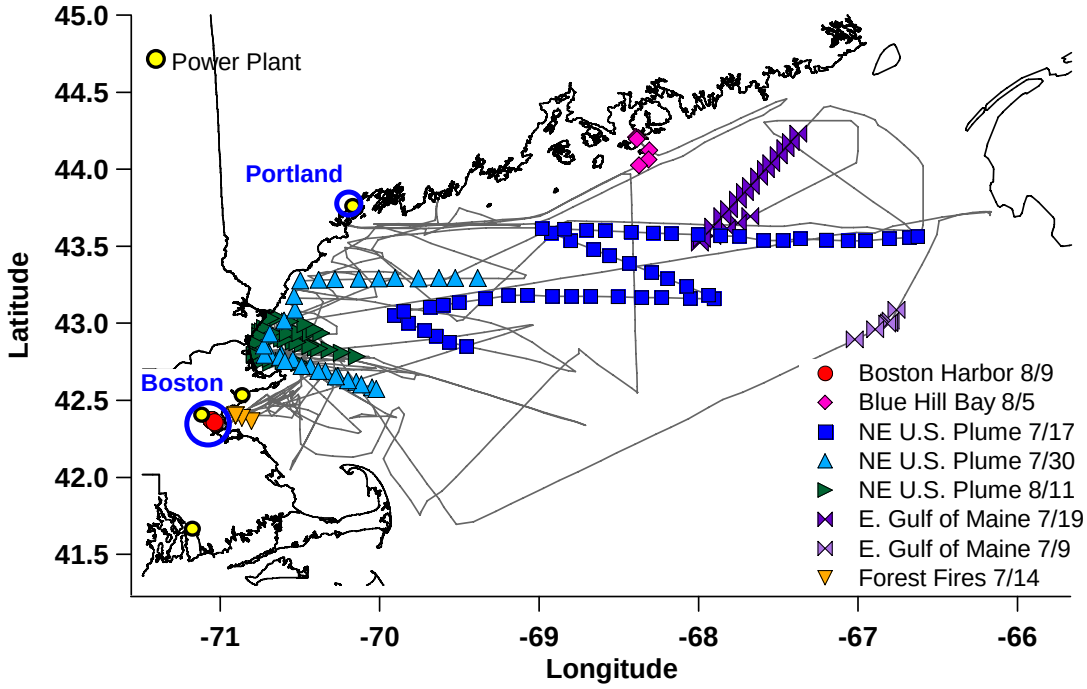

Figure 2. Boston Harbor. a) Cruise track as the ship entered Boston Harbor. Wind barbs indicate the local wind direction. Track and wind barbs are colored as a function of the toluene concentration in ppbv. b) F_O and m44/POM and c) NR POM, toluene, benzene, toluene to benzene ratio, and insolation as the ship sat in Boston Harbor.

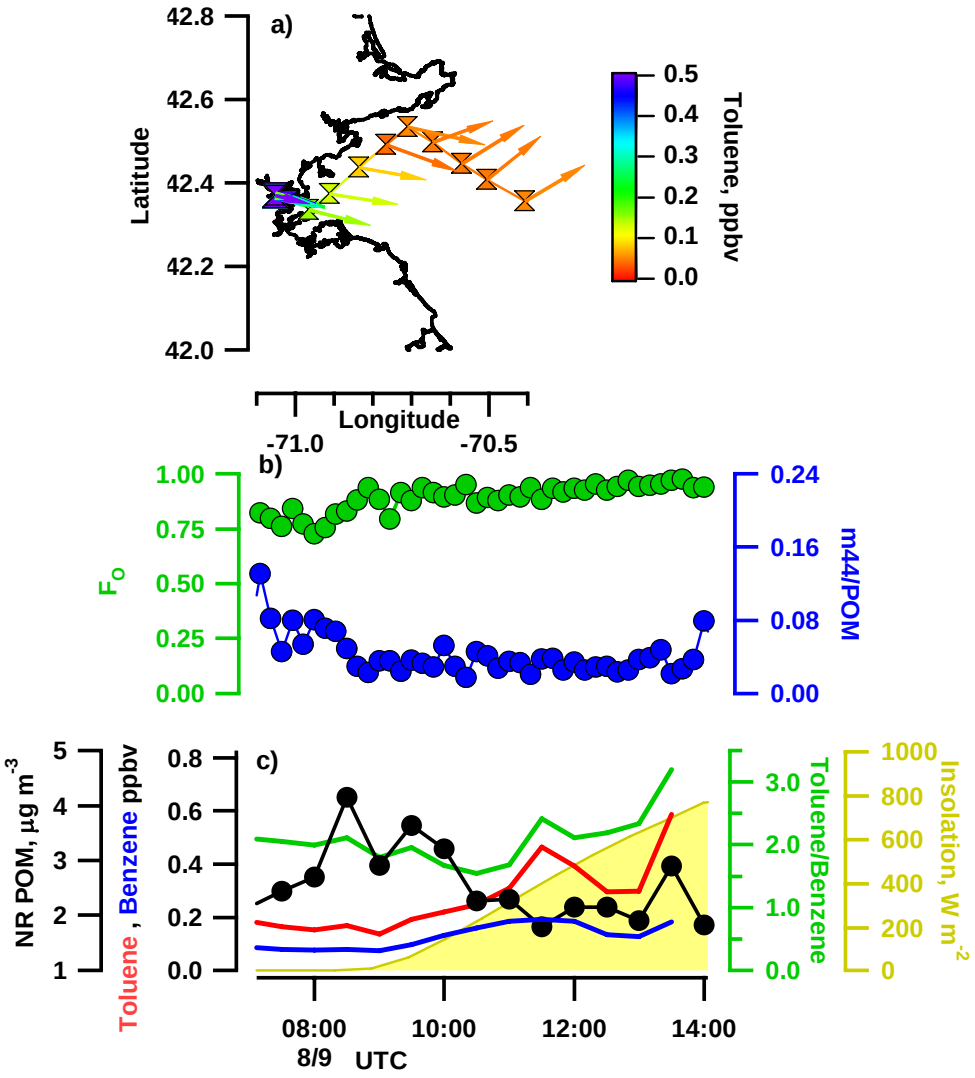

Figure 3. Blue Hill Bay, Acadia National Park. a) Cruise track as the ship entered the bay. Wind barbs indicate the local wind direction. Track and wind barbs are colored as a function of the sum of measured monoterpenes. b) F_O and m44/POM and c) NR POM, iso-propyl nitrate, sum of measured monoterpenes, MPAN, and insolation as the ship sat in Blue Hill Bay.

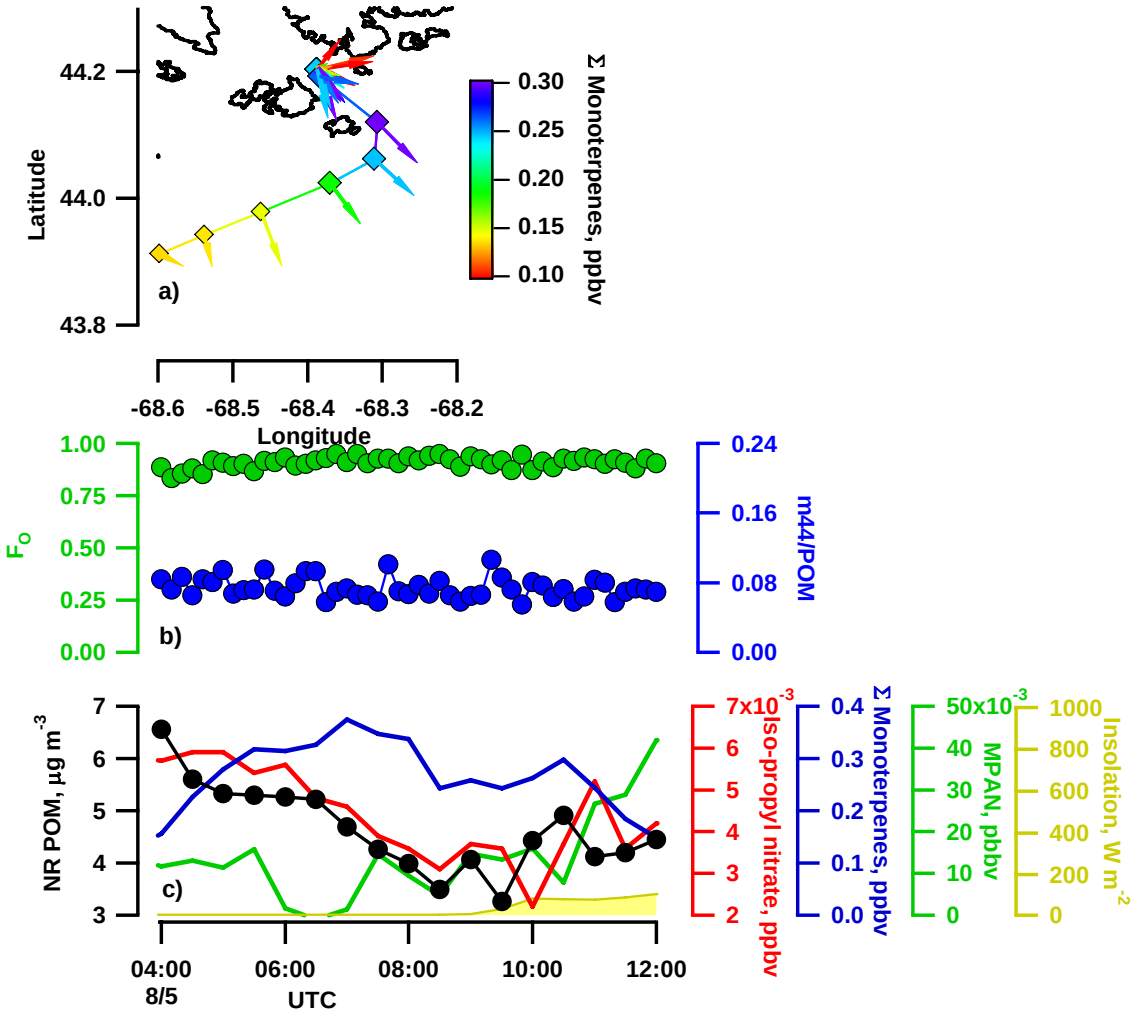

Figure 4. MPAN and iso-propyl nitrate versus NR POM as the ship sat in Blue Hill Bay (8/5 04:00 to 10:00 UTC).

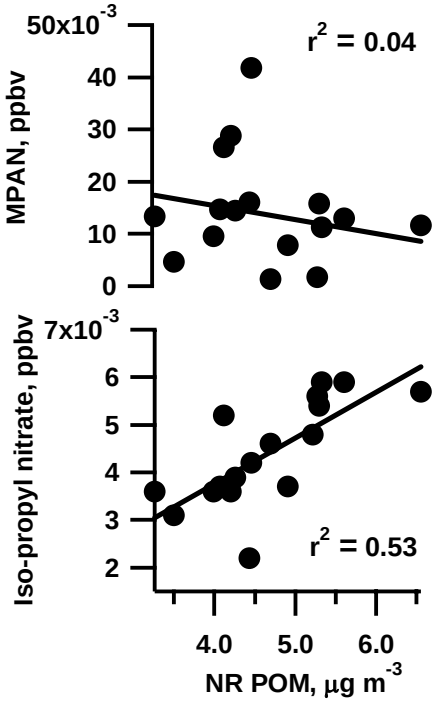

Figure 5. Sub-1 μm scattering coefficient (Mm^{-1}) for the entire cruise with periods of NE U.S. plume case studies highlighted (top panel). Bottom panel shows Flexpart footprint PES with sampling end times of 7/17/04 1952, 7/30/04 1958, and 8/11 1830 UTC. Numbers superimposed on the footprint plots indicate approximate location of the plume in days back in time.

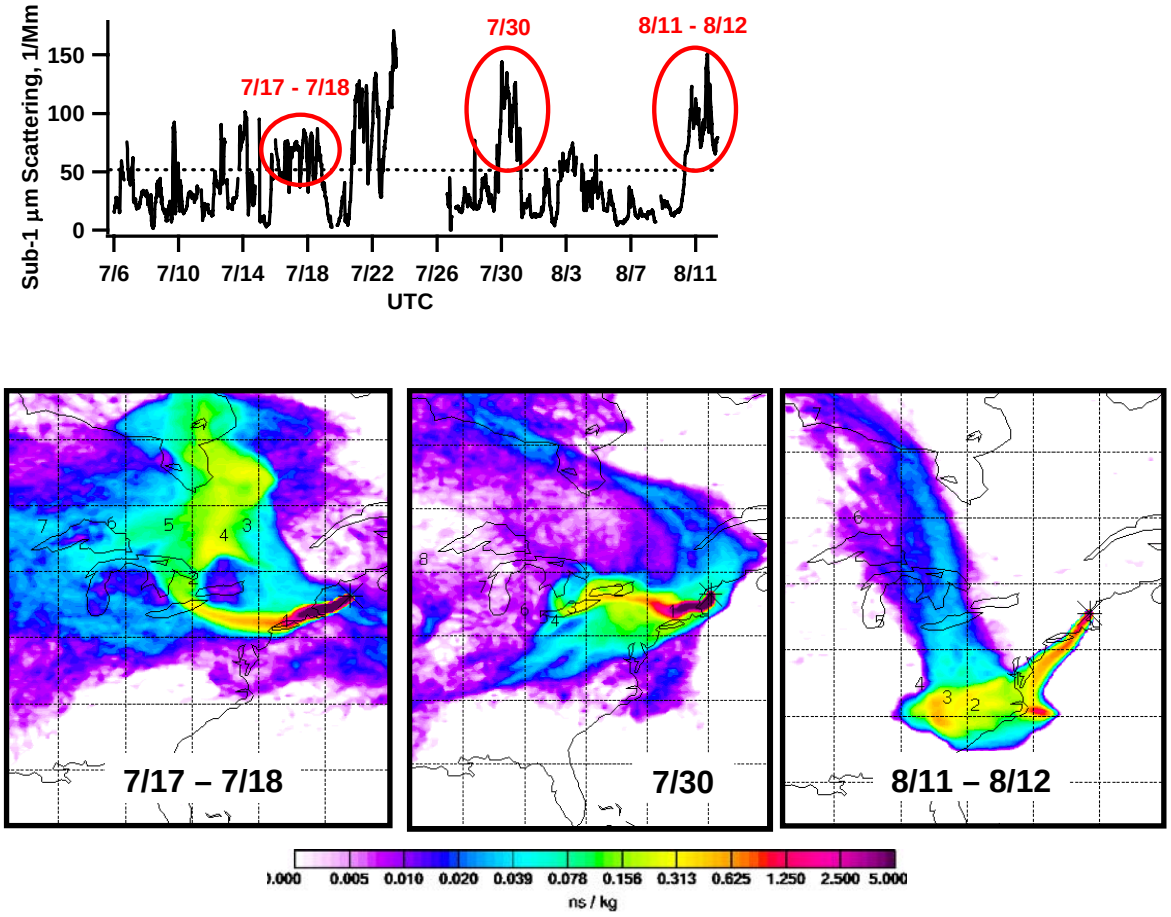

Figure 6. NE U.S. urban plume 7/17 – 7/18. a) Cruise track through the plume colored as a function of sub-1 μm scattering. b) F_O, ER, F_{SO4}, m44/POM, and Longitude. Dashed lines are linear fits to the time series of F_O (green), ER (pink), and m44/POM (blue) and c) NR POM, toluene, benzene, the toluene to benzene ratio, and iso-propyl nitrate along the cruise track.

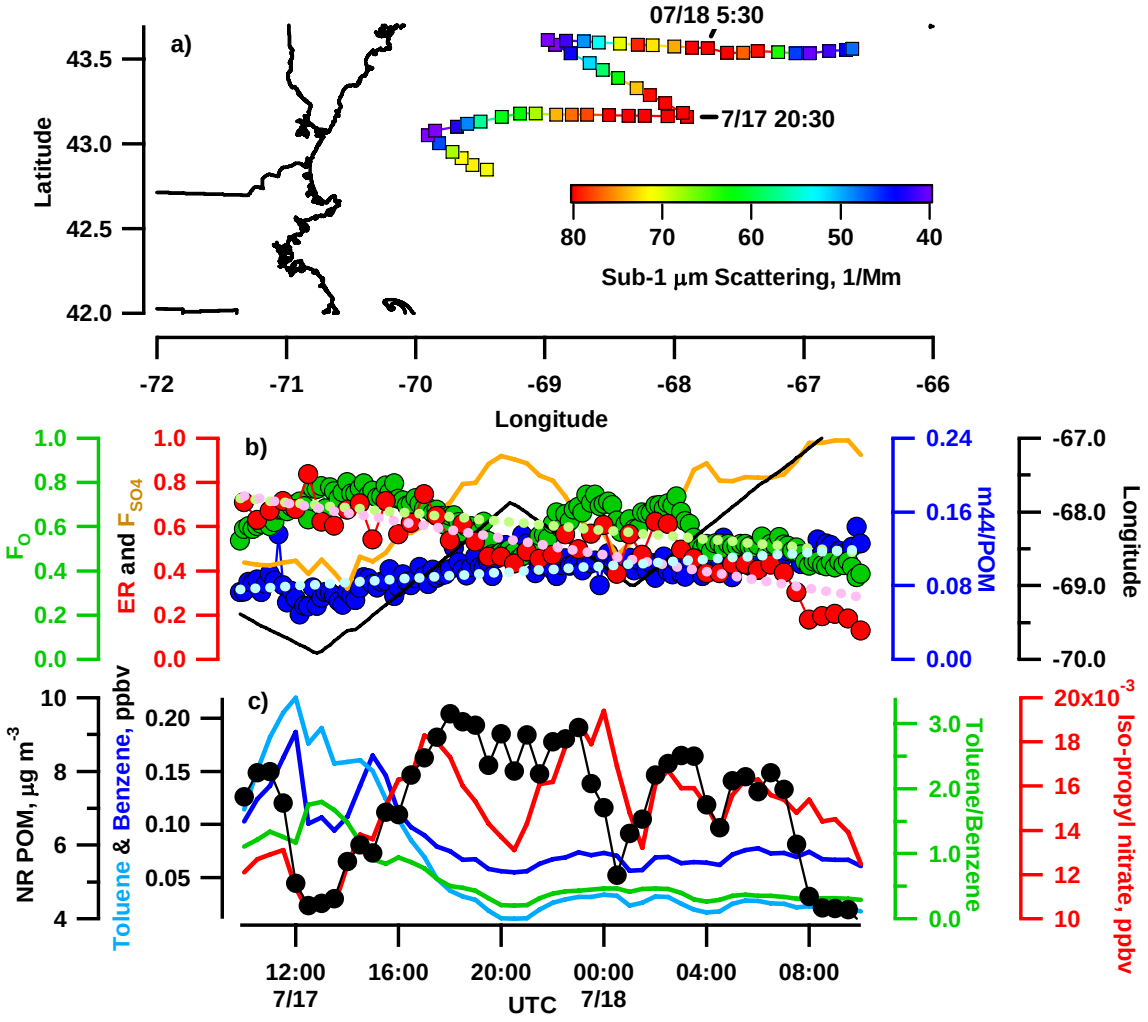

Figure 7. Time series of the “Flexpart Transport Clock” which gives the age spectra of anthropogenic American emissions based on backward simulations. Shown are the composite ages of CO, SO_2, and NO_2 tracers (all in ppbv) for the a) 7/17 to 7/18, b) 7/30, c) 8/11 to 8/12, d) 7/9, and e) 7/18 to 7/19 case studies.

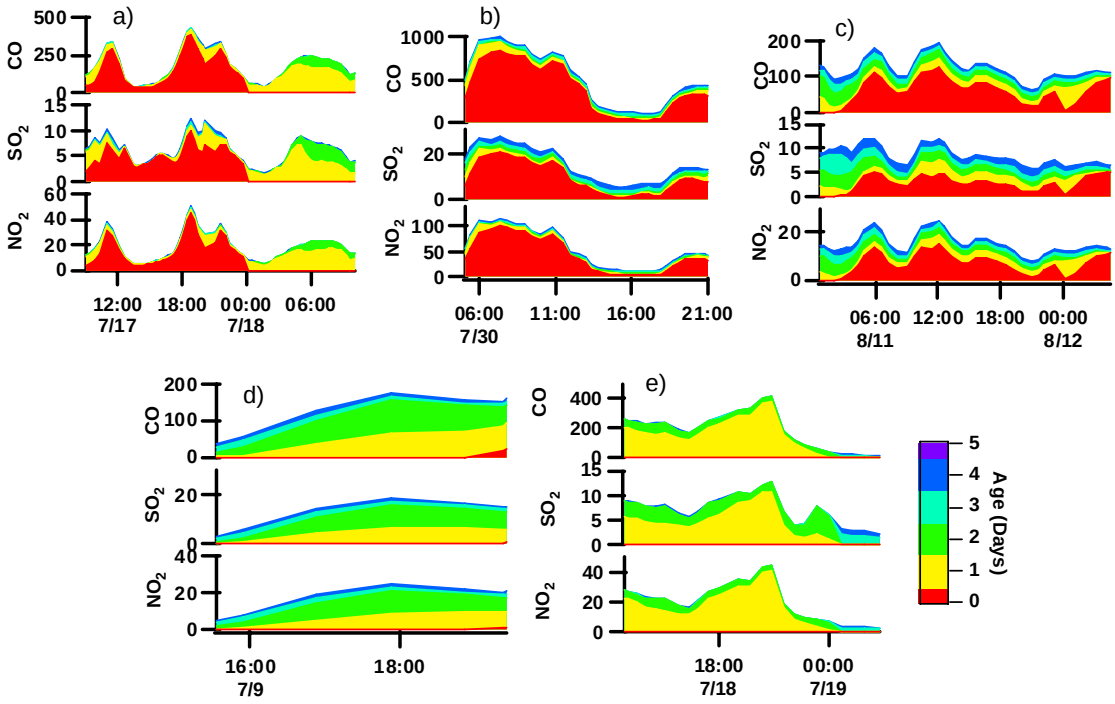

Figure 8. NE U.S. urban plume 7/30. a) Cruise track through the plume colored as a function of sub-1 μm scattering where yellow dots represent the location of power plants. b) F_O, ER, F_{SO4}, m44/POM, and Longitude and c) NR POM, toluene, benzene, the toluene to benzene ratio, and iso-propyl nitrate along the cruise track.

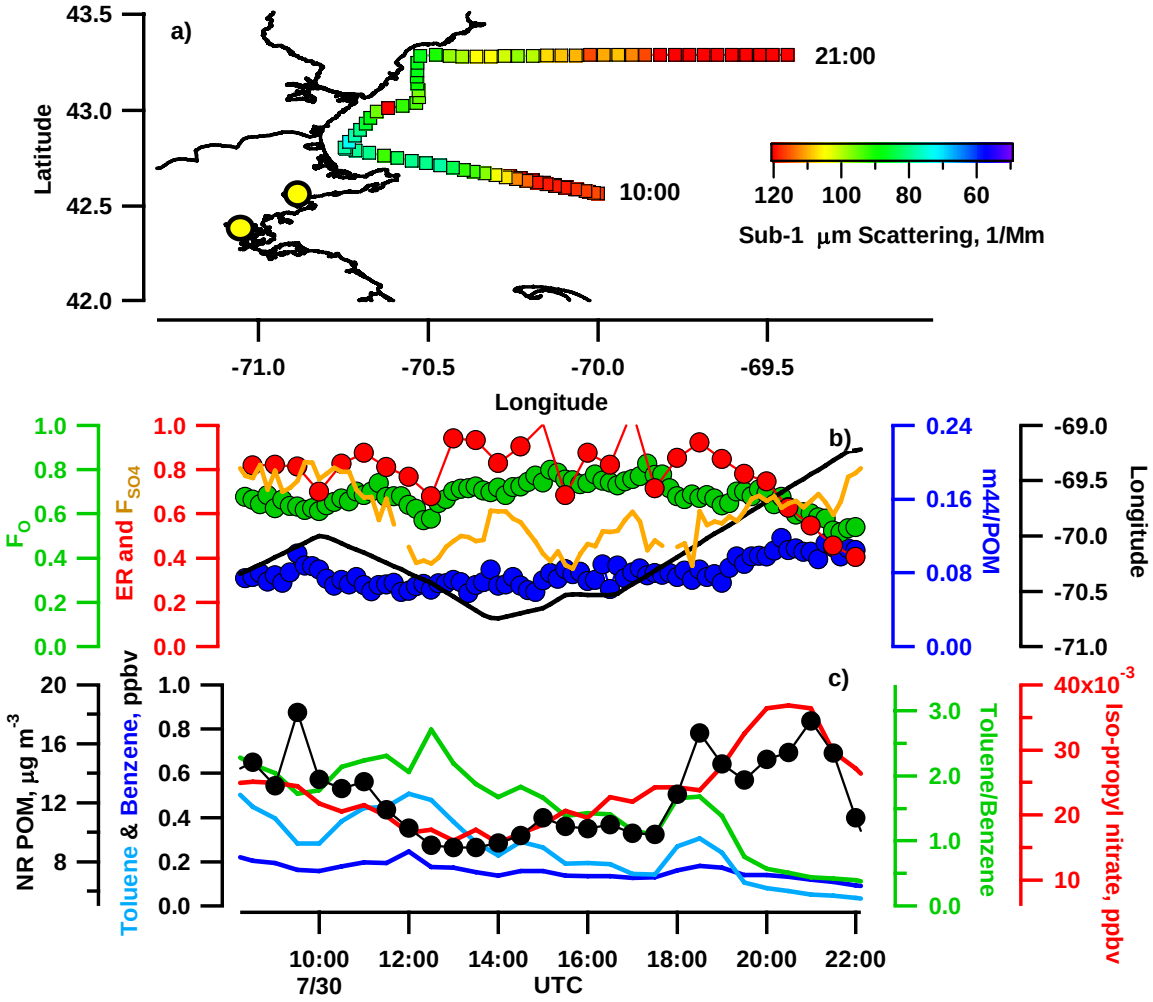

Figure 9. NE U.S. urban plume 8/11 – 8/12. a) Cruise track through the plume colored as a function of sub-1 μm scattering. Yellow dots indicate location of power plants. b) F_O, ER, F_{SO4}, m44/POM, and longitude and c) NR POM, toluene, benzene, the toluene to benzene ratio, and iso-propyl nitrate along the cruise track.

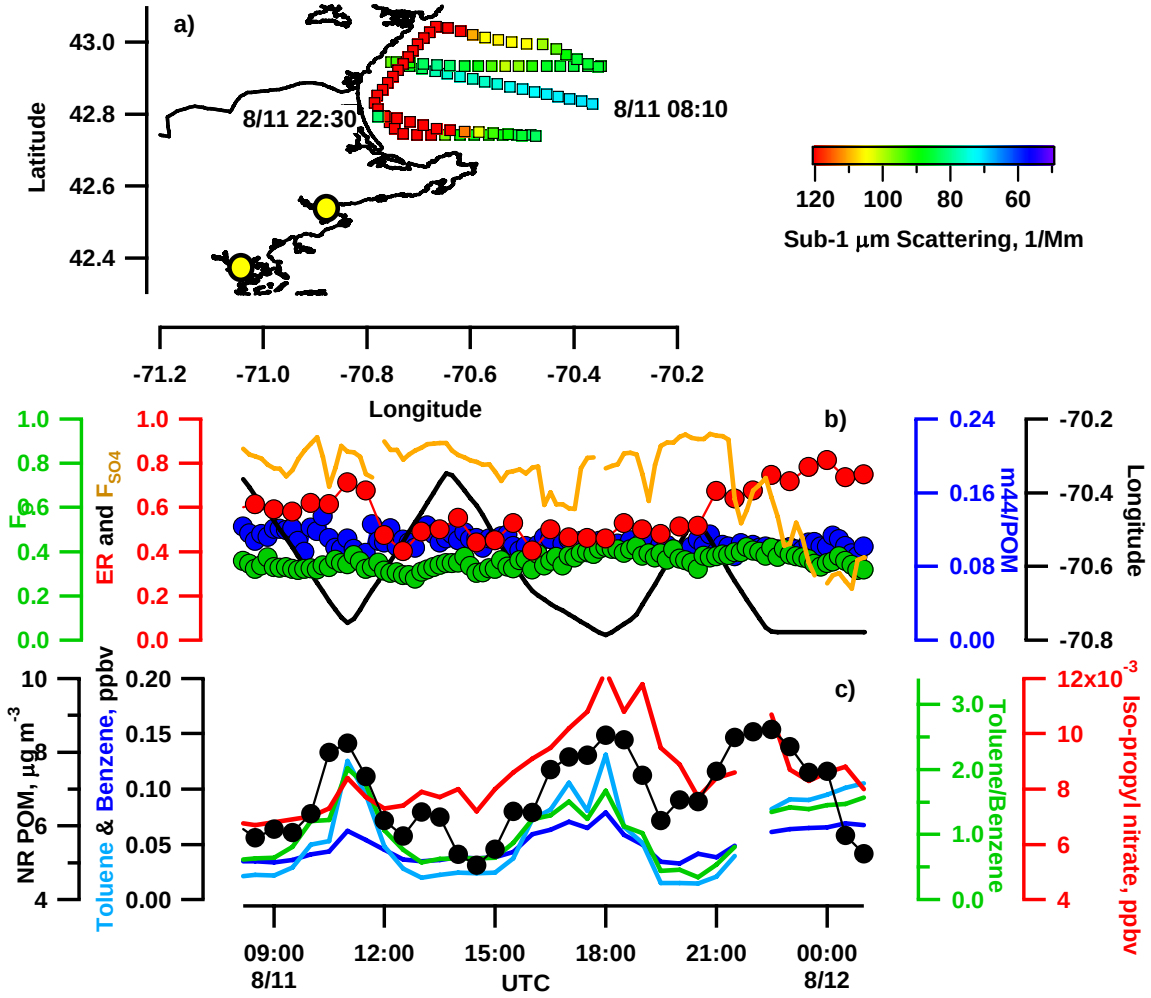

Figure 10. FLEXPART footprint PES with sampling end times of 7/09/04 16:53, 7/18 14:35, and 7/19 02:55 UTC. Numbers superimposed on the footprint plots indicate approximate location of the plume in days back in time.

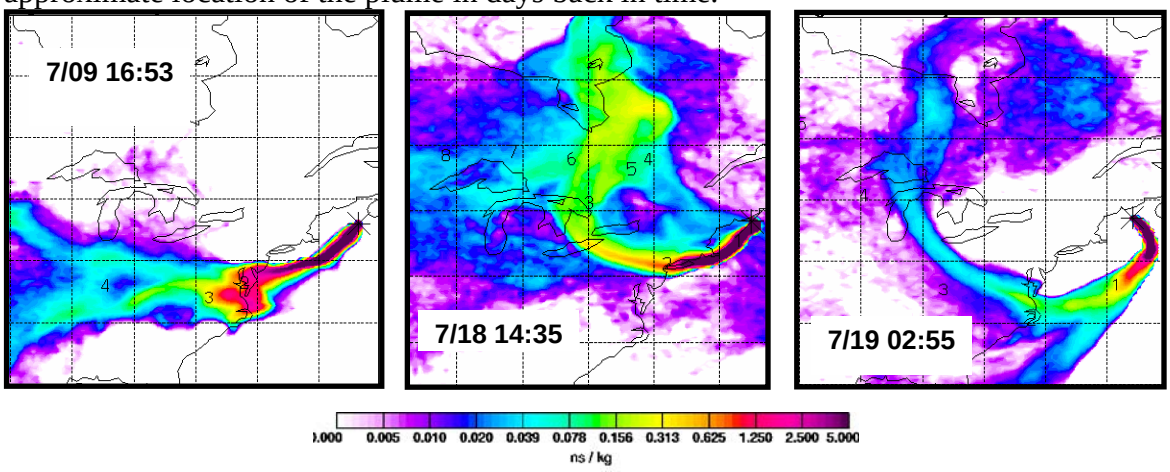

Figure 11. E. Gulf of Maine, 7/9. a) Cruise track through the plume colored as a function of sub-1 μm scattering, b) F_O, ER, F_{SO4}, and m44/POM, c) NR POM, toluene, benzene, the toluene to benzene ratio, and iso-propyl nitrate along the cruise track.

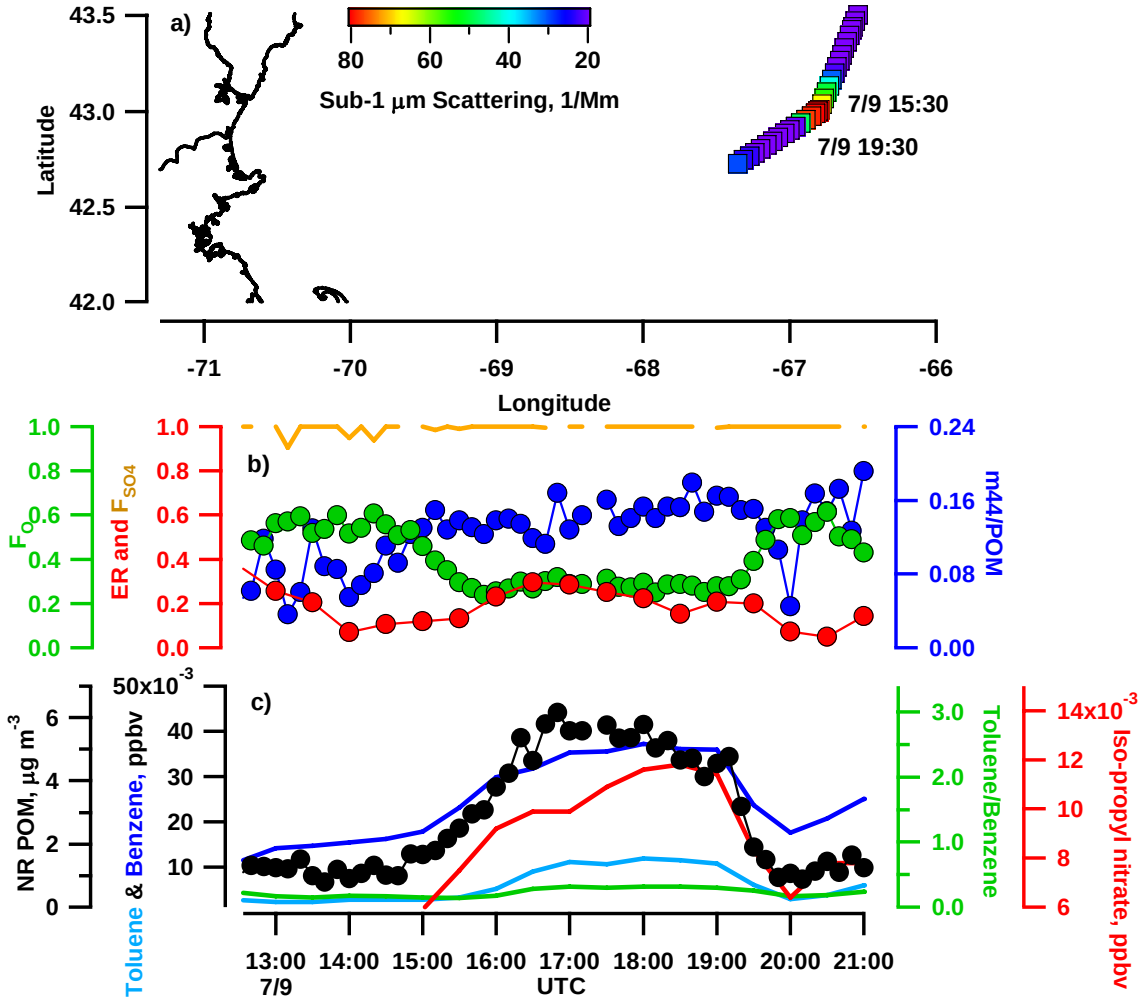

Figure 12. E. Gulf of Maine, 7/19. a) Cruise track through photochemically younger (7/18 12:00 – 16:00 UTC indicated by squares) and older (7/19 00:00 – 04:00 UTC indicated by circles) air masses colored as a function of the toluene to benzene ratio, b) F_O, ER, F_{SO4}, and m44/POM, and c) NR POM, the toluene to benzene ratio, and iso-propyl nitrate along the cruise track.

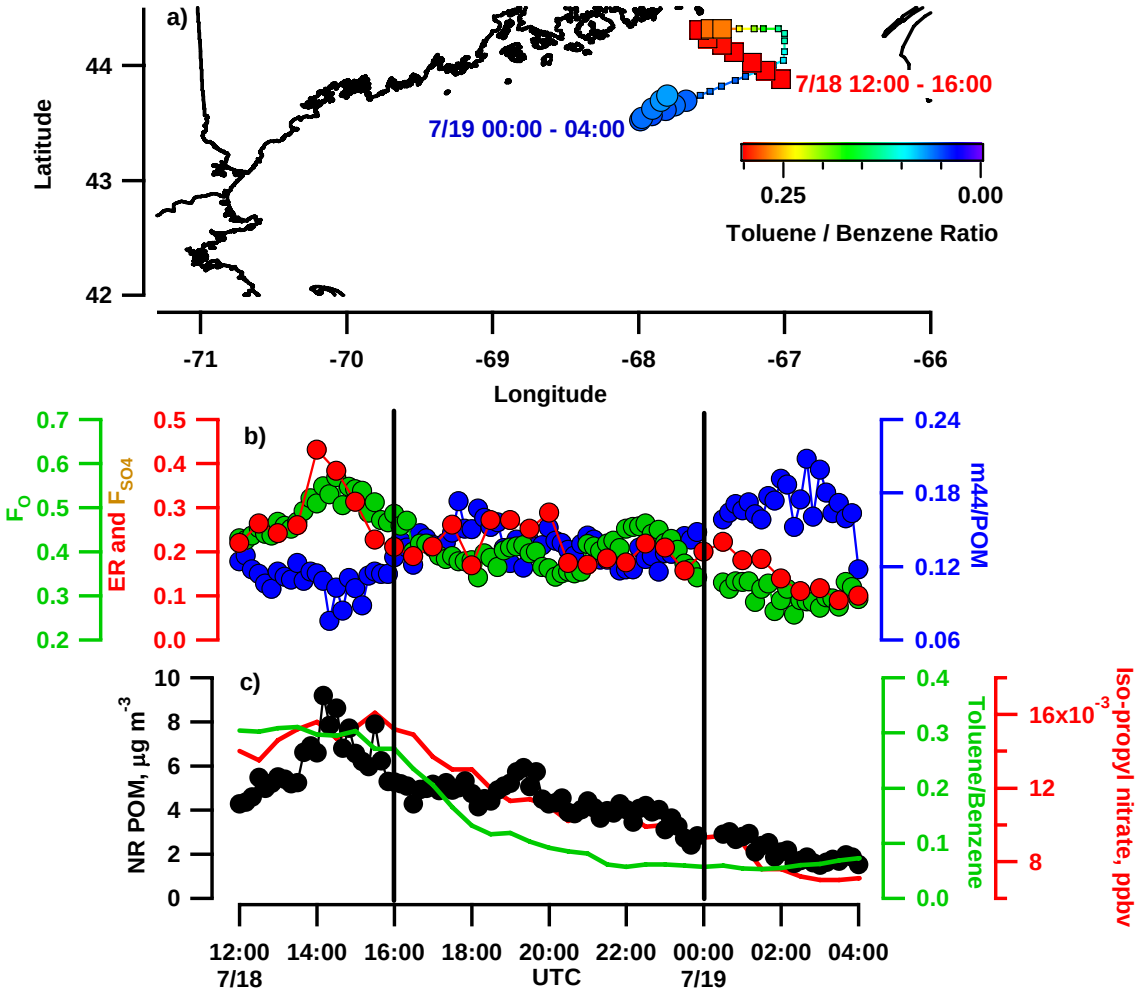

Figure 13. N. American forest fires, 7/14/04. a) Cruise track and wind barbs colored as a function of the acetonitrile concentration. Large symbols indicate measurement period shown in b) and c). b) F_O and m44/POM and c) NR POM, acetonitrile, the toluene to benzene ratio, and iso-propyl nitrate along the cruise track.

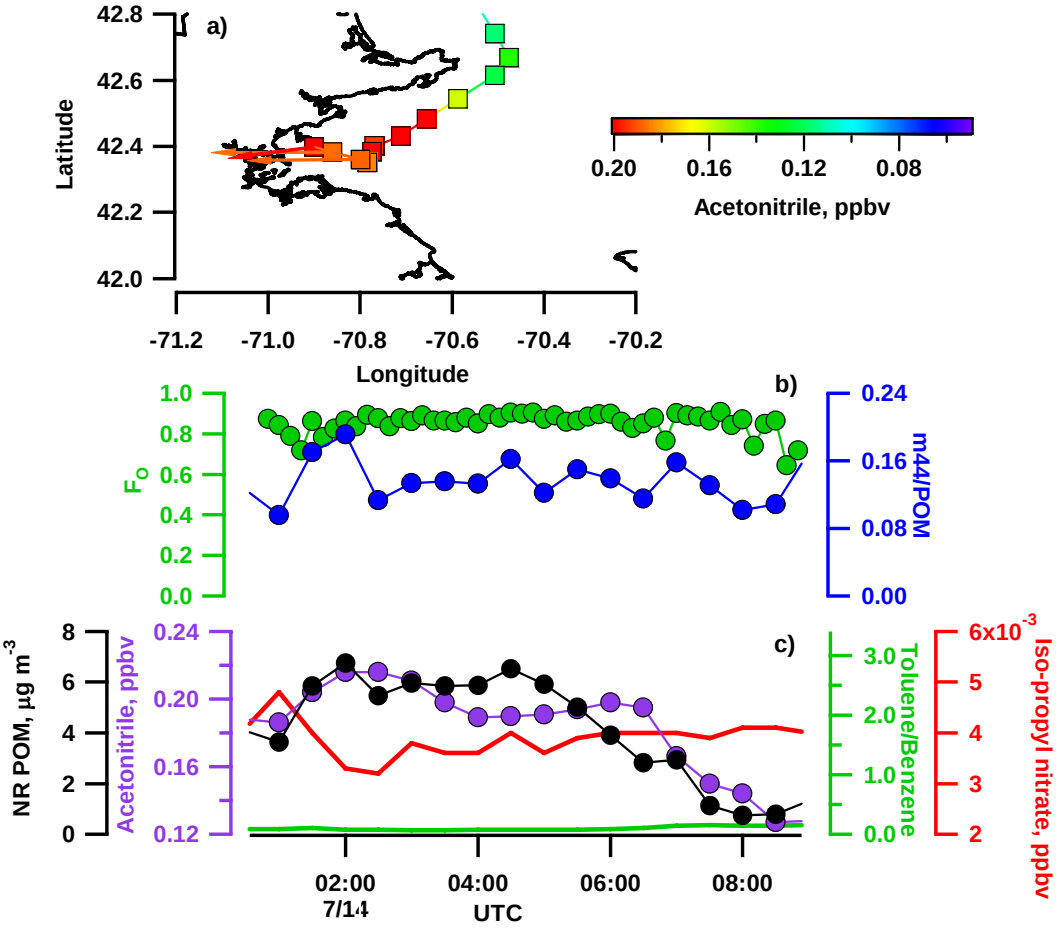

Figure 14. FLEXPART column integrated PES for the sampling end time of 7/14/04 03:25 UTC. Fire hot spots detected by the MODIS instruments on board the AQUA and TERRA satellites between 1 and 10 July are indicated as black dots.

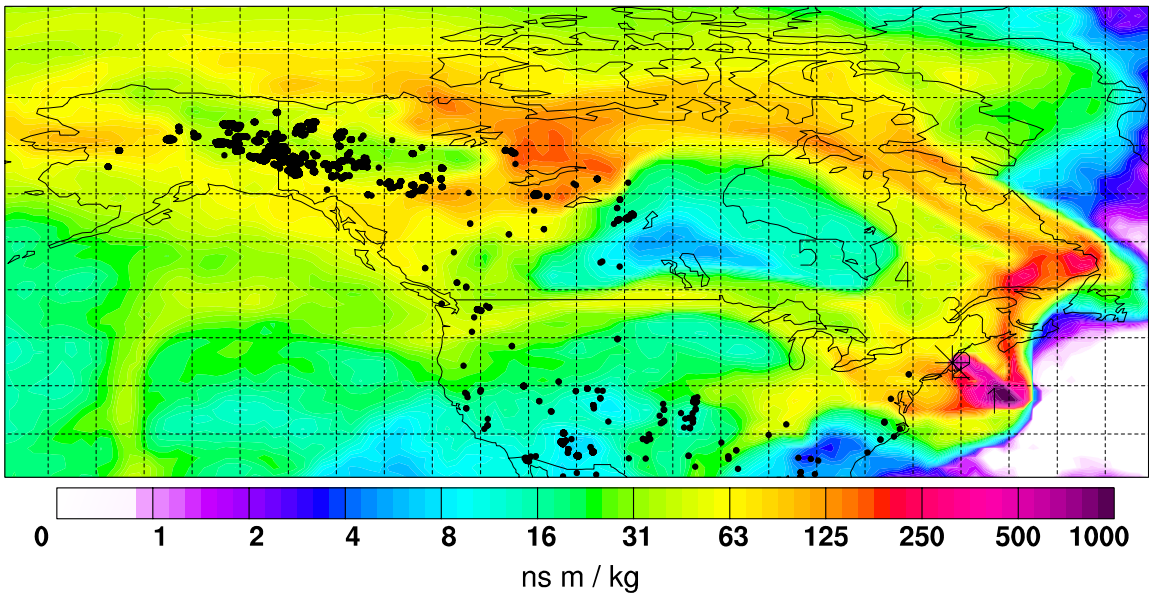

Figure 15. $f_{\sigma ep}(66, 30)$ versus F_O. Open circles include all data points from the cruise. The heavy solid line represents the linear fit to all data, the dashed lines show the 95% confidence level for the fit, and the lighter solid lines show the 95% prediction bands. Data points from the case studies are highlighted.

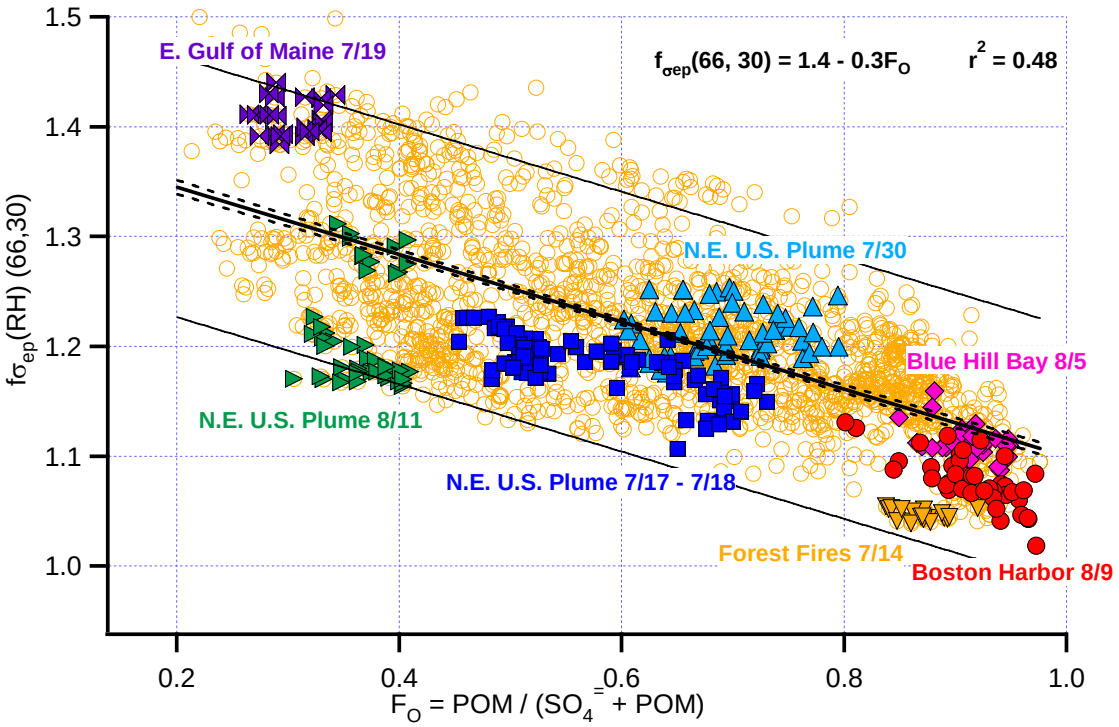

Figure 16. $f_{\sigma ep}(66, 30)$ versus F_O. Symbols are colored according to equivalence ratio Data points from the case studies are shown. The linear fit to all data pates also is shown as in Figure 15.

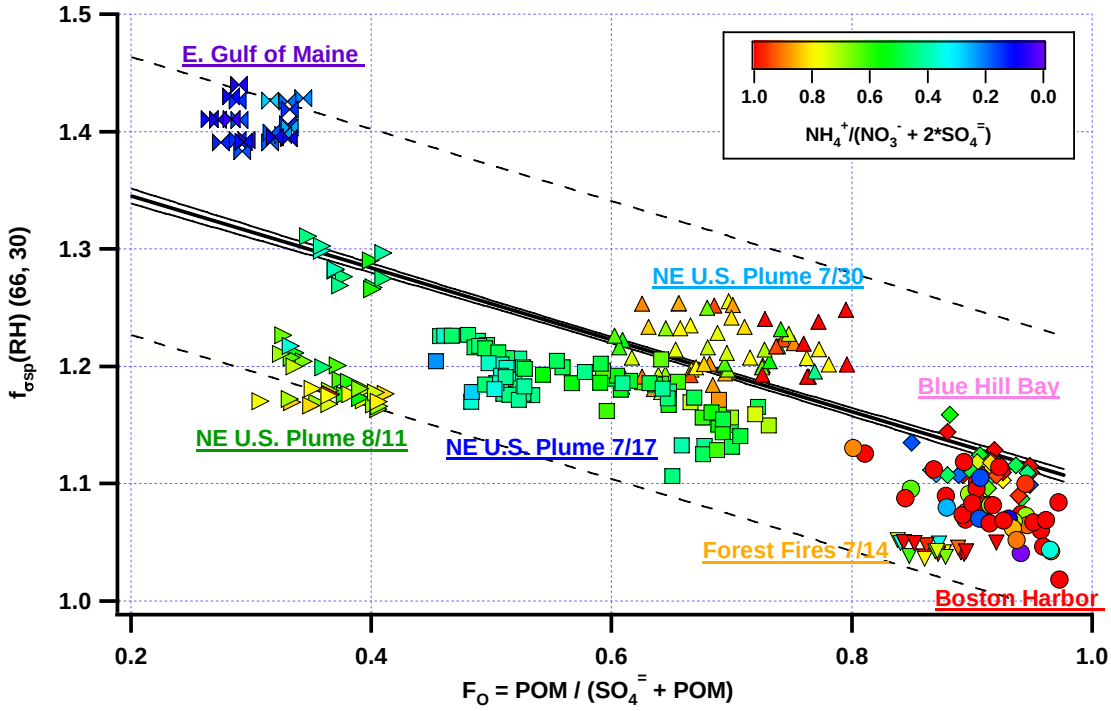

Figure 17. $f_{\sigma ep}(66, 30)$ versus F_O. Symbols are colored according to the m44/POM ratio. Data points from the case studies are shown. The linear fit to all data pates also is shown as in Figure 15.

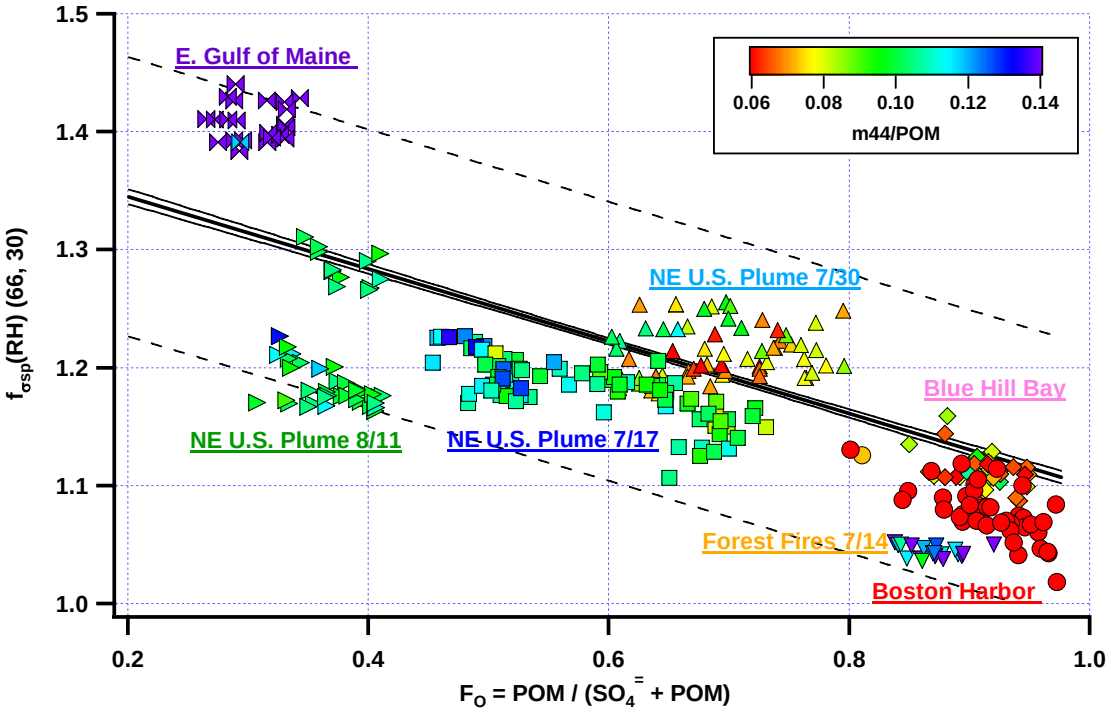

Figure 18. $f_{\sigma ep}(66, 30)$ versus F_O. Symbols are colored according to the geometric mean surface diameter. Data points from the case studies are shown. The linear fit to all data pates also is shown as in Figure 15.